Tight oil sandstones in Upper Triassic Yanchang Formation, Ordos Basin, N. China: Reservoir quality destruction in a closed diagenetic system

Mingjie Liu[1], Jon Gluyas[2], Weibin Wang[3, 4], Zhen Liu[5], Junbang Liu[6], Xiucheng Tan[1], Wei Zeng[1], Yi Xiong[7]

[1] School of Geoscience and Technology, Southwest Petroleum University, Chengdu, 610500, China

[2] Department of Earth Sciences, Durham University, Durham, DH1 3LE, UK

[3] Research Institute of Exploration and Development, PetroChina Changqing Oil Field Company, Xi'an 710018, China

[4] National Engineering Laboratory for Exploration and Development of Low-Permeability Oil & Gas Fields, PetroChina, Xi'an 710018, China

[5] College of Geosciences, China University of Petroleum, Beijing, 102249, China

[6] Research Institute of Petroleum Exploration and Development, PetroChina, Beijing 100083, China

[7] School of Geosciences, Yangtze University, Wuhan, 430100, China

Correspondence

Mingjie Liu, School of Geoscience and Technology, Southwest Petroleum University, No. 8, Xindu Road, Xindu District, Chengdu 610500, China. E-mail: liumingjieldd@163.com

Funding information. Natural Science Foundation of China (Grant No. 41502147, Grant No. 41672124), China Postdoctoral Science Foundation (Grant No. 2016M600752), Sichuan Province Education Department Foundation (Grant No. 16ZA0072), National science and technology major project of China (Grant No. 2016ZX05047001-002)

ABSTRACT

An investigation of the Triassic Yanchang Formation, Ordos Basin, N. China, revealed that the diagenesis and quality of tight oil sandstone reservoirs (with an average porosity of 9.83% and an average permeability of 0.96 mD) were controlled by a

closed diagenetic system. The carbonate cements observed in the sandstone were derived from decarboxylation of organic matter that occurred in the adjacent mudstones. These reactions supplied CO_3^{2-} which reacted with cations derived from grain dissolution in the sandstones. The average size of the diagenetic geochemical system with respect to carbonate cements was small ($<6 \times 10^{-2} m^3$), comprising sandstone and its adjacent mudstone(s). The carbonate cements tend to concentrate in the marginal sandstone which is taken to indicate that the flux of CO_3^{2-} into the sandstones limited the quantity of carbonate precipitated. In addition, the mass near balance between the amount of feldspar dissolution and its byproducts in the central sandstone (distance to the sandstone/mudstone interface is mainly more than 1 m), where the permeability of sandstone will present a decrease trend with the increasing of feldspar dissolution pores. The pore space of central sandstone will be just redistributed, with primary intergranular pores converting to feldspar dissolution pores and clay minerals micropores. Thus, the best part of the sandstone reservoirs tends to be the central part of sandstone. In particular, sandstones that are more than 2 m thick could be the potential hydrocarbon reservoirs because they retain the best porosity (average of 13.6%) and permeability (average of 1.8 mD). The results of our study provide an important guide for the exploration of tight oil sandstones in other petroliferous basins over the world.

KEYWORDS

closed diagenetic geochemical system; Ordos Basin; reservoir quality; tight oil sandstone; Yanchang Formation

1 INTRODUCTION

It is now widely believed that the quality of sandstone reservoir is controlled by the original depositional characteristics and diagenesis (Dutton & Loucks, 2010; Ehrenberg, 1990; Gluyas & Coleman, 1992; Higgs, Zwingmann, Reyes, & Funnell, 2007; Mansurbeg et al., 2009; Morad, Ketzer, & DeRos, 2000; Taylor et al., 2010). Various integrated approaches and cases have been given to analyze how the

sandstone reservoir quality is controlled by the diagenesis (Gier, Worden, Jones, & Kurzweil, 2008; Maast, Jahren, & Bjørlykke, 2011; Umar, Friis, Khan, Kassi, & Kasi, 2011; Yuan et al., 2015a; Zhang, Pe-piper, & Piper, 2015). However, most of the studies are based mainly on the description of diagenesis, with only a little consideration given to the geochemical constraints on the diagenetic system (Bjørlykke & Jahren, 2012; Chuhan, Bjørlykke, & Lowrey, 2001; Yuan et al., 2015b; Yuan, Cao, Zhang, & Gluyas, 2017). Essentially, the dissolution and precipitation of minerals are chemical reactions, with their extent and rates controlled by a combination of temperature, pore-water composition and some parameters such as redox potential (Eh) and acidity (pH). These processes make up the "the geochemical system", which can be divided into open system and closed system according to the exchange characteristics of diagenetic materials (Bjørlykke & Jahren, 2012). Although some detailed papers have been published to investigate the relationship between the open/closed geochemical system and diagenesis, their mainly focused on the conventional sandstone and mudstone, not including the tight sandstone (Bjørlykke & Jahren, 2012; Chuhan et al., 2001; Day-Stirrat et al., 2010; Yuan et al., 2015b; 2017).

As one of the most important unconventional hydrocarbon resources, the tight sandstones have been found widely distributed in the petroliferous basins of the world in recent decades (Higgs et al., 2007; Schmitt et al., 2015; Spencer, 1985), especially in China, such as the Ordos Basin, Sichuan Basin, Bohai Bay Basin and Songliao Basin (Liu et al., 2014; Liu, Liu, Wu, Zhu, & Wang, 2017; Xi et al., 2015a; Zou et al., 2012a). Generally, a tight sandstone is defined as a sandstone with porosity lower than 10%, the air permeability lower than 1mD (Law & Curtis, 2002; Spencer, 1985; Stroker, Harris, Crawford Elliott, & Marion Wampler, 2013; Xi et al., 2015a ; Zou et al., 2010a). The Upper Triassic Yanchang Formation is a prolific oil-producing unit of the Ordos Basin (Fu et al., 2017; Guo et al., 2012; Yang, Li, & Liu, 2013; Yao et al., 2013). Diagenesis of the tight sandstone in Yanchang Formation has been reported in some published works, most of which are focused on the Chang 7 Member (e.g., Cui et al., 2017; Dou, Liu, Wu, Xu, & Feng, 2017; Wu et al., 2016; Zhang, Bao, Zhao,

Jiang, & Gong, 2017; Zhu et al., 2015). However, limited attention has been paid to the Chang 8 Member (Liu, Liu, Wang, & Pan, 2016; Wang, Chang, Yin, Li, & Song, 2017; Zhou et al., 2016), as well as the relationship between diagenesis and reservoir quality based on the diagenetic geochemical system. Additionally, although the effects of diagenetic alterations have been well studied to provide valuable interpretations for tight sandstone reservoir quality, difficulties remain when applying the present results to predict the "sweet zones" of anomalously high porosity and permeability within the tight sandstone reservoirs of Chang 8 Member.

The good core coverage of tight oil sandstone in Xifeng oilfield provides an excellent opportunity to investigate this problem. In this paper, we take a combined analysis of petrography, porosity and permeability, stable isotopic compositions of authigenic minerals, homogenization temperature and final ice melting temperature of aqueous fluid inclusion and pore water chemistry, aimed to: (1) investigate a detailed diagenetic analysis and reconstruct the diagenetic history of Chang 8 Member tight sandstone; (2) identify the type of diagenetic geochemical system; and (3) analyze the control of the diagenetic geochemical system on the tight sandstone reservoir quality in Chang 8 Member.

2 GEOLOGICAL BACKGROUND

The Ordos Basin, as the second largest sedimentary basin in China, locates in the western part of the North China Block and covers approximately 320 000 km^2 (Figure 1 A) (Liu et al., 2004; Yang, Jin, Van Loon, Han, & Fan, 2017). It is a typical cratonic basin characterized by gentle, west-dipping monocline with dip angles less than 1° (Figure 1 B) (He, 2003; Liu et al., 2014; Wang et al., 2017). Six first-order tectonic units in the Ordos Basin have been identified, i.e., the Yimeng Uplift in the north, the Western Thrust Belt on the west margin, the Tianhuan Depression in the west, the Yishan Slope in the center, the Weibei Uplift in the south and the Jinxi Fault-Fold Belt in the east (Figure 1 C) (Liu et al., 2016; Yang, 2002). The studied Xifeng Area, as one of the most oil-rich areas, belongs to the Yishan Slope and locates in the

south-western part of the Ordos Basin. Based on the filling sequence and structures, the Ordos Basin evolution can be divided into five stages: (1) an aulacogen stage during the Middle-Late Proterozoic, (2) a shallow oceanic platform stage during the Early Palaeozoic, (3) an offshore plain stage during the Late Palaeozoic, (4) a lacustrine basin stage during the Mesozoic, and (5) a peripheral fault depression stage during the Cenozoic (Xu et al., 2017; Yang, Liu, Zhang, Han, & Hui, 2007).

During the Late Triassic, the Yanchang Formation is dominated by fluvial, lacustrine and deltaic sedimentation with a thickness of 1000–1300 m throughout most of the Ordos Basin (Figure 2) (Cui et al., 2017; Qiu, Liu, Wang, Deng, & Mao, 2015; Zou, Wang, Li, Tao, & Hou, 2012b). Recent hydrocarbon exploration and outcrop studies have demonstrated that shallow-lacustrine sand-rich deltas developed extensively along the gentle slopes and central part of the basin, forming the main reservoir rocks of the Triassic oil fields (Zhou et al., 2016). The vertical facies succession indicates that the Yanchang Formation covers the entire lacustrine life cycle of the Late Triassic Ordos Basin (Figure 2) (Zou et al., 2010b).

Based on the sedimentary cycle, rock associations, tuff marker beds and log characteristics, the Yanchang Formation is divided into ten members, numbered from top to bottom as Chang 1 to Chang 10 (Figure 2) (He, 2003; Yang, 2002; Yang et al., 2017). Lake-basin development peaked during the deposition of Chang 7 Member, simultaneously peaked in the development of Mesozoic hydrocarbon source rocks with an average total organic carbon (TOC) of 13.75% and a vitrinite reflectance (Ro) in the range of 0.85–1.15% (Yang & Zhang, 2005; Zhang, Yang, Li, & Ma, 2006). The overlying Chang 6 Member and underlying Chang 8 Member are the main reservoir beds of Yanchang Formation tight sandstone hydrocarbon reservoirs (Liu et al., 2014; Zhang, Yang, Hou, & Liu, 2009). This study focused on the Chang 8 Member of Xifeng Area, in which oil is mainly accumulated in the sandstones of shallow lacustrine delta distributary channel (Zhou et al., 2016).

Burial history and thermal history of the Xifeng Area have been analyzed in detail using data from exploration and production wells and the histories synthesized with the BasinMod software by previous studies (Guo et al., 2012; Liu et al., 2013;

Ren et al., 2007). The current geothermal gradient is about 29.3 ℃/km, with an average surface temperature of 10.8 ℃. Presently, the Yanchang Formation is not at its maximum depth (~3 km) and temperature (130 ℃).

3 DATABASES AND METHODS

This study involved the analysis of 268 thin-section samples from 60 wells, 1073 reservoir porosity and permeability measurements and 40 formation water data. Samples and data were collected from the PetroChina Research Institute of Petroleum Exploration & Development and PetroChina Changqing Oilfield Company.

All the sandstone samples were selected from the Chang 8 Member drill cores of 60 wells according to the study objectives and constraints of the collected data. A total of 158 thin sections and 110 blue epoxy resin-impregnated thin sections were prepared for the analysis of rock mineralogy, diagenesis and visual porosity. Thin sections were partly stained with Alizarin Red S and K-ferricyanide for carbonate mineral identification. Point counts were performed on thin sections for the content of detrital grains with at least 300 points, following the method of Yuan et al. (2015a, b). 20 micrographs for each of 59 blue epoxy resin-impregnated thin sections were taken using the Leica microscope in the Key Laboratory of Natural Gas Geology of Southwest Petroleum University, Sichuan Province, in order to determining the content of quartz cement, carbonate cements, authigenic clays, primary pores and the feldspar dissolution pores. Objectives of 100× for these thin sections were used, and each micrograph has an area of 6.45mm^2 (Xi et al., 2015a, b). Then cements and pores in each micrograph were identified under the microscope and sketched by using the CorelDRAW software on computer. The total area of cements and pores in every micrograph was obtained using the Image-Pro Plus software. Finally, the percentages of cements and pores were calculated by taking the average of all values in the 20 micrographs for each thin section. Besides, a total of 59 sandstone samples were analyzed for whole-rock (bulk) and clay fraction (＜2 μm) mineralogy using XRD in the State Key Laboratory of Oil and Gas Reservoir Geology and Exploitation of

Southwest Petroleum University.

59 typical samples were identified using a Quanta 250 FEG scanning electron microscope (SEM) equipped with an energy dispersive X-ray spectrometer (EDX) in the State Key Laboratory of Oil and Gas Reservoir Geology and Exploitation of Southwest Petroleum University. Cathodoluminescence (CL) analyses of 14 representative samples were made using a Leica microscope equipped with a CL8200-MK5 CL instrument in the Key Laboratory of Natural Gas Geology of Southwest Petroleum University, Sichuan Province. Twenty core samples from 20 wells were prepared as thick doubly-polished thin sections for fluid inclusion petrographic analysis and microthermometric measurements in the Key Laboratory of Natural Gas Geology of Southwest Petroleum University, Sichuan Province. The microthermometry of fluid inclusions was studied using a petrographic microscope equipped with a Linkam THMSG 600 heating and cooling stage which enables to transfer the temperatures of phase in the range of -180 to 500 ℃. The measured precision for the homogenization temperature (T_h) and ice melting temperature (T_m) are ± 1 °C and ± 0.1 °C, respectively.

Based on the petrological studies, 59 organic matter-free sandstone samples were chosen for carbon and oxygen stable isotope analysis. These samples were analyzed using a Thermo-Finnigan MAT 253 isotope ratio mass spectrometer in the Key Laboratory of Natural Gas Geology of Southwest Petroleum University, Sichuan Province, with measured precision was ± 0.08‰ for O and ±0.06‰ for C. Carbon and oxygen stable isotope data are reported in parts per thousand relative to the Vienna PeeDee Belemnite (V-PDB) standards.

4 RESULTS

4.1 Reservoir lithologies

Petrographic investigation of the tight sandstones in Chang 8 Member shows that the detrital components contain 18.7–64.3% quartz (avg. 38.3%), 5.4–56.5% feldspars (avg. 31.5%) and 5.2–63.1% rock fragments (avg. 30.2%), mostly lithic arkoses and

feldspathic litharenites (Figure 3). In the studied tight sandstones, the majority of the detrital quartz grains are monocrystalline. The detrital feldspars are mainly plagioclase and altered K-feldspar. The rock fragments primarily consist of volcanic rock fragments with an average of 19.4%, sedimentary rock fragments with an average of 2.8%, metamorphic rock fragments with an average of 6.7%, and mica with an average of 1.3%. According to the grading analysis, the studied tight sandstones in Chang 8 Member are fine-medium grained, with moderate to well sorting, and the roundness of detrital grains varies from subangular to subrounded. The grain contacts are dominated by linear contacts and concavo-convex contacts.

4.2 Reservoir properties

In general, the reservoir properties of the tight sandstones in Chang 8 Member are quite poor. It decreases with increasing burial depth from 1500 m to 3000 m (Figure 4A, B), with the porosity and permeability showing a positive correlation relationship (Figure 4C).The tight sandstones in Chang 8 Member have a range of porosity from 1.2% to 18.74% (mainly 4.0% to 16.0%) with an average of 9.83% (Figure 4D). Horizontal permeability ranges from 0.003 to 56.29 mD (mainly less than 1 mD) with an average of 0.96 mD (Figure 4E).

4.3 Diagenetic mineralogy

Authigenic minerals in the tight sandstones of Chang 8 Member mainly consist of quartz, carbonate cements and clay minerals. The authigenic quartz and clays are usually associated with altered feldspar.

4.3.1 Quartz cement

Authigenic quartz is evident in the thin sections and SEM, mainly occurring in two different types of morphologies: quartz overgrowths and authigenic quartz crystals. The quartz overgrowths are easy to discriminate from the detrital grains, with the dust clay rims on the grains in thin sections (Figure 5A) and the euhedral hexagonal pyramid quartz crystal on the grains in SEM (Figure 5B). The authigenic quartz

crystals can be identified by the intergranular pore-filling euhedral hexagonal pyramid quartz crystal both in thin sections and SEM (Figure 5C, D). In the studied tight sandstone, the authigenic quartz is difficult to distinguish from the detrital quartz in CL, due to the quartz grain and quartz cement all are dark non-luminescent (Figure 5E, F). As a whole, the authigenic quartz in the tight sandstones of Chang 8 Member was no more than 1% of the whole rock and showed insignificant trend with the burial depth increasing (Figure 6A).

4.3.2 Feldspar dissolution

The feldspar dissolution, especially detrital K-feldspar, is common in the tight sandstone reservoirs of Chang 8 Member, resulting in the formation of significant secondary intragranular pores during the burial stage (Figure 5G). Generally, feldspar dissolution is always accompanied by the precipitation of albite, authigenic quartz crystal and illite (Figure 5H, I), which are the byproducts of feldspar dissolution. The absolute contents of feldspar dissolution obtained from the thin sections ranges from 0.81% to 3.63% (avg. 1.78%) of the whole rock, showing no significant trend with increasing burial depth (Figure 6B).

4.3.3 Carbonate cements

Four types of carbonate cements (calcite, dolomite, ferrocalcite and ankerite) have been identified in the tight sandstone of Chang 8 Member. Calcite cements and dolomite cements mainly occur as pore-filling blocky crystals between detrital grains (Figure 7A), and the calcite cements also show a bright orange luminescence color in CL (Figure 7B, C). In addition, the dolomite cements occur as scattered euhedral rhombs and partly fill the intergranular pores (Figure 7D). In thin sections, the ferrocalcite cements and ankerite cements also occur as pore-filling blocky crystals. They mainly filled in the pores around the euhedral authigenic quartz crystal (Figure 7E, F), replaced the quartz grain and dolomite cements (Figure 7F-H) and filled the feldspar dissolution pores completely (Figure 7H, I). It indicated that the ferrocalcite and ankerite cements formed after the quartz cement, dolomite cement and feldspar

dissolution. As a whole, the content of carbonate cements in the tight sandstone reservoirs of Chang 8 Member is in the range of 0.1–36% (avg. 7.1%), showing no significant trend with increasing burial depth (Figure 6C).

4.3.4 Clay minerals

Based on the XRD and SEM analysis, various types of clay minerals with different amounts and textural habits are identified in the studied tight sandstone reservoirs. The kaolinite, illite and chlorite are the most important types of authigenic clays. The smectite and mixed-layer illite/smectite (I/S) are the minor clay minerals in the tight sandstone of Chang 8 Member. These clay minerals are generally filling the primary and secondary pores with different textural habits, for example, the kaolinite primarily occurs as booklets and vermicular aggregates (Figure 8A, B), the smectite occurs as curly flakes (Figure 8C), the mixed-layer illite/smectite (I/S) mainly occurs as foliated or honeycomb aggregates (Figure 8D) and the illite occurs as fibrous and sometimes honeycomb-textured masses (Figure 8E, F). In addition, the rosette-shaped and needle-shaped chlorite occurs mainly as coatings and rims covering the framework grain and authigenic quartz crystal (Figure 8 G-I). According the texture relationship, two stages of chlorite are found in the studied tight sandstone reservoirs, the stage-I chlorite formed before calcite and the stage-II chlorite formed after authigenic quartz.

In general, the kaolinite, illite, and chlorite in the tight sandstone reservoirs of Chang 8 Member accounts for 1.4–51.2% (avg. 16.7%), 7–79% (avg. 34.6%) and 16.7–60.9% (avg. 45.2%) of the total clay content, respectively. In addition, the kaolinite mainly exists at the depth shallower than about 2100 m, and reduces below the depth (Figure 6D), where temperatures exceed to 110 °C. On of contrary, the percentage of illite increases quickly at a depth deeper than about 2300 m, showing an increase trend with increasing burial depth (Figure 6E). The content of chlorite displays a slight increasing trend with the increasing burial depth (Figure 6F).

4.4 Isotopic composition of carbonate cements

59 tight sandstone samples were chosen for the isotopic composition analysis of

carbonate cements, and the details of all types and contents are summarized in Table 1. Most calcite and dolomite have a relatively wide range of $\delta^{18}O$ values from -20.78‰ to -10.89‰ (avg. -15.11‰) and $\delta^{13}C$ from -10.23‰ to 1‰ (avg. -5.97‰). Ferrocalcite and ankerite have a range of $\delta^{18}O$ values from -22.11‰ to -16.75‰ (avg. -19.73‰) and $\delta^{13}C$ from -9.85‰ to -0.66‰ (avg. -4.96‰).

4.5 Fluid inclusions

The aqueous inclusions with a diameter about 2-12 μm, commonly present in the quartz overgrowths, authigenic quartz crystals and carbonate cements in the tight sandstone reservoirs of Chang 8 Member. Most of them are two-phase inclusions and have gas bubbles at room temperature.

The measured homogenization temperatures (T_h) and final ice melting temperature (T_m) of the aqueous inclusions in this study are shown in Table 2. Figure 9 presents the T_h distribution of aqueous inclusions in the quartz cements, including overgrowths and authigenic quartz crystals. The formation temperature of carbonate cements can be obtained both by the T_h of aqueous inclusions and the approximate precipitation temperatures calculated by the oxygen isotope for all the studied samples (Table 1). The aqueous inclusions in quartz overgrowths and authigenic quartz crystals yield T_h ranges mainly from 77.3 ℃ to 123.5℃ and from 71℃ to 90℃, respectively. The T_h of the aqueous inclusions in carbonate cements ranging mainly from 51.7 ℃ to 117.8 ℃. Meantime, the calculated precipitation temperatures for the calcite/dolomite and the ferrocalcite/ankerite are in the range of 49.03–110.57 ℃ and 79.93–140.32 ℃, respectively.

4.6 Pore water

40 pore-water samples were measured from the tight sandstone reservoirs of Chang 8 Member. It indicated that approximately 73.3% characterized by $CaCl_2$ water, 13.3% characterized by $MgCl_2$ water, 6.7% characterized by Na_2SO_4 water, and 6.7% characterized by $NaHCO_3$ water. Generally, the salinity of pore water is high in these samples, ranging from 3.2 g/L to 70.8 g/L. It shows an increasing trend with the burial

depth increasing, as well as the ion concentrations in the different solutes mentioned above (Figure 10).

5 DISCUSSION

5.1 Sources of carbonate cements

Previous studies have suggested that there were three potential sources of carbonate cements in the sandstone, including the external source (from adjacent mudstones or source rocks, etc.), the internal source (e.g. locally reprecipitated detrital carbonate grains or bioclasts), or a mixing of both (Dutton & Loucks, 2010; Gier et al., 2008). In the tight sandstone reservoirs of Chang 8 Member, provenance evidences and petrological feature show no occurrence of detrital carbonate grains and bioclasts, indicating the carbonate cement should derive from the external source.

The $\delta^{13}C$ value of carbonate cements in the tight sandstone of Chang 8 Member is in the range of -10.2–1‰, representing a single carbon source from the decarboxylation of organic matter in the adjacent mudstone/source rocks (Figure 11A; Irwin, Curtis, & Coleman, 1977). In addition, the $\delta^{13}C$ value increases with the increasing distance of sample to the source rocks (Figure 11B), which indicating the origin of carbonate cements were also controlled by the decarboxylation of organic matter in the adjacent mudstones/source rocks (Xi et al., 2015a).

Previous studies have established that the ions of Ca^{2+}, Mg^{2+} and Fe^{2+} can be provided by the conversion of volcanic rock fragments (Boles & Franks, 1979; Stroker et al., 2013). As mentioned above, a large amount of unstable volcanic rock fragments exists in the studied tight sandstone. In addition, the porosity of mudstones in Chang 7 Member generally evolved from nearly 40% to mainly less than 10% at present (Liu et al., 2012). During such a period, large amounts of advective compaction fluids with Ca^{2+}, Mg^{2+} and Fe^{2+} were expelled from the mudstones to the adjacent sandstones (Bjørlykke & Jahren, 2012; Xi et al., 2015a). As a result, the concentrations of these ions are higher along the sandstone/mudstone interface than in the central part of the sandstone body. When these ions mixed with the CO_3^{2-} which

derived from the organic matter decarboxylation in the adjacent mudstone, the initial physical and chemical equilibrium is broken, allowing the carbonate to precipitate (Dutton & Loucks, 2010; Milliken & Land, 1993). In this situation, the carbonate cements preferentially concentrated in the marginal sandstone, showing a decrease trend with the increasing distance to the sandstone/mudstone interface (Figure 12A).

5.2 Sources of quartz and authigenic clay minerals

In general, the concentrations of SiO_2 (aq) and Al^{3+} are extremely low in the pore water of sandstone (Bjørlykke & Jahren, 2012, Xi et al., 2015a; Yuan et al., 2015a), Due to the constraints of water volume and considerable heterogeneity in porosity and permeability, the SiO_2 (aq) and Al^{3+} are difficult to transfer for a long distance from the mudstone to the adjacent sandstone through advective flow, thermal convection or diffusion, especially with the overlying mudstone of Chang 7 Member develops overpressure (Bjørlykke & Jahren, 2012; Liu et al., 2012). However, the content of quartz cements and authigenic clay minerals in the studied tight sandstone decreases towards the sandstone/mudstone interface (Figure 12B, C), indicating that the quartz cement and clay minerals in the tight sandstone reservoirs of Chang 8 Member should originate from an internal source.

As the studied sandstones experienced the minimal dissolution pressure, it is impossible that the quartz comes from the pressure dissolution. In addition, the petrological observations from thin sections show that the quartz cements and authigenic clays are always accompanied with feldspar dissolution pores (Figure 5I), suggesting that the quartz cements and clay minerals are the byproducts of feldspar dissolution. Furthermore, the positive relationship between the feldspar dissolution porosity and content of clay/quartz cement (Figure 13A, B), also indicates that the feldspar dissolution provides the source to quartz cements and authigenic clay minerals, which is consistent with the results of previous studies (Giles & De Boer, 1990; Higgs et al., 2007; Yuan et al., 2015a).

5.3 Diagenetic sequence

Aqueous inclusions can provide valuable information for the precipitation temperature of authigenic minerals (Robinson & Gluyas, 1992). In this study, the homogenization temperatures (T_h) of fluid inclusions (including the precipitation temperatures calculating by oxygen isotope values of carbonate cements, and the T_h of fluid inclusions in quartz and carbonate cements) and texture relationship can be used to infer the relative timing of major diagenetic sequence and reconstruct the diagenetic history of the tight sandstone reservoirs in Chang 8 Member.

The T_h of aqueous inclusions ranges from 71℃ to 123.5℃ in the quartz cements with an average of 97.4℃, and from 41.03℃ to 140.32℃ in the carbonate cements. However, two T_h peaks of aqueous inclusions have been observed in the carbonate cements, mainly ranging from 50℃ to 70℃ and 100℃ to 130℃ (Figure 9), which suggests that there are two stages of carbonate cementation. The dolomite cements were always replaced by the ferrocalcite and ankerite, and the ferrocalcite and ankerite cements mainly filled in the pores around the euhedral authigenic quartz crystal (Figure 7E-H). It indicates that the dolomite and quartz cements formed before the ferrocalcite and ankerite cements. Therefore, the two T_h peaks of carbonate cements are respectively correspond to the T_h of calcite/dolomite and ferrocalcite/ankerite. In addition, the calcite mainly cemented the point-linear contact grains (Figure 7A, 8H), indicating an early stage of diagenesis when cementation occurred. Moreover, there is no authigenic quartz replaced by calcite/dolomite cement. As a result, based on the T_h of fluid inclusions in carbonate and quartz cements, it is inferred that the authigenic quartz cement formed later than the early carbonate cement (calcite/dolomite) and earlier than the late carbonate cement (ferrocalcite/ankerite).

As a whole, with the constraints of petrographic evidences described above (Figure 5, 7, 8), the source analysis of related diagenetic minerals, and the burial-thermal history of well Xi17 in Xifeng Area, the diagenetic sequence of Chang 8 Member tight sandstone can be summarized in Figure 14.

5.4 Types of diagenetic geochemical system

The salinity of pore water shows an increase trend with the burial depth increases (Figure 10), suggesting limited advective mixing of pore waters from different origins (Bjørlykke & Gran, 1994; Bjørlykke & Jahren, 2012). Since the studied sandstone escaped the near-surface water quickly with rapid burial (Figure 14), it indicates little impact of meteoric water after deposition. The overlying Chang 7 Member commonly developed moderate to strong fluid overpressure with few faults, which can strongly reduce the penetration of meteoric water in Chang 8 Member (Liu et al., 2012). It is consistent with the result that there is little impact of meteoric water due to the overlying overpressure (Bjørlykke, 1993; Yuan et al., 2015b). Moreover, a large number of authigenic illite formed when burial depth was greater than 2300m (Figure 6D), at the moment the temperature was about 120℃ (Figure 14). In such a situation, the concentration of K^+ in the pore water from Chang 8 Member tight sandstone is in the range of 0.019–1.1g/L (Figure 10), most of which were greater than 0.12g/L (the minimum concentration of K^+ for illitization when the temperature >120℃) (Bjørlykke, 1998). Thus, the concentration of K^+ can promote the illitization of kaolinite and K-feldspar. Therefore, it can be concluded that enough K^+ should have retained in the studied tight sandstone systems because of the occurrence of illitization reactions, which indicates a closed geochemical system during the diagenesis.

In addition, the salinity of pore water during the diagenesis can be calculated by the ice melting temperature (T_m) of aqueous fluid inclusions in the quartz cements and carbonate cements (Table 2). It is in the range of 3.55–20.67%, mostly greater than 10%, showing an increasing trend with the burial depth increasing (Figure 15). Moreover, the contents of carbonate cements, quartz cements, authigenic clay minerals and feldspar dissolution pores show slightly variation within the sandstone when the distance to the sandstone/mudstone interface more than 1m (Figure 12 A-D). These above phenomena all indicated that there is less mass transfer between the internal and external environment during the diagenesis. Thus, it can be concluded that the tight sandstone of Chang 8 Member should be in a closed geochemical system.

Furthermore, from the petrological evidences, the authigenic quartz and clay minerals, as the byproducts always accompanied with feldspar dissolution, without long-distance transportation. It is also consistent with a closed geochemical system. Therefore, combining the analysis of petrographic texture relationship, distribution pattern of authigenic minerals and feldspar dissolution, characteristics of pore water, salinity of diagenetic fluid and geologic setting of Xifeng Area, it suggests that the geochemical system is closed during the diagenesis of Chang 8 Member tight sandstone reservoir.

5.5 Effects of diagenetic geochemical system on tight sandstone reservoir quality

As the tight sandstone reservoirs of Chang 8 Member were in a closed geochemical system during the diagenesis, the diagenetic mass could not effectively transport in the pore water to exchange with the external materials (Bjørlykke & Jahren, 2012). Thus, the diagenetic reactions including mineral dissolution and precipitation always occur in a confined space, in where the authigenic quartz and clay minerals cements result from feldspar dissolution are always exist together with the dissolution pores within the studied tight sandstone (Figure 5I). Generally, the feldspar dissolution could improve the reservoir quality, however, the cementation of quartz and clay minerals have a negative impact on the porosity and permeability of tight sandstone. In addition, due to the closed diagenetic system, the carbonate cements preferentially concentrated in the marginal sandstones (distance to the sandstone/mudstone interface mainly less than 1 m), preventing the external pore water with CO_3^{2-} ion from flowing to the central sandstone (Figure 12A).

In order to analyze the diagenetic process of feldspar dissolution and how its precipitated byproducts simultaneously affect the sandstone porosity, the content of feldspar dissolution pores, clay and quartz cement can be evaluated in the thin sections (Yuan et al., 2015b). The difference value between the feldspar dissolution porosity and the sum of byproducts in Chang 8 Member is in the range of -1.07–1.03% (avg. 0.07%) (Figure 16), which means the minerals alternation has little impact on the absolute porosity of sandstone reservoir in the diagenetic process under a closed

system. Besides, the porosity of core samples shows an insignificant trend with the increasing feldspar dissolution porosity (Figure 17A). Although the feldspar dissolution releases some pore space, its byproducts occupy some primary intergranular pore as well, which means the pore space is just redistributed from the primary intergranular pores converting to the feldspar dissolution pores and clay minerals micropores (Giles & De Boer, 1990; Yuan et al., 2015b). Meantime, the permeability of the studied tight sandstone shows a decreasing trend with the proportion of dissolved feldspar increasing (Figure 17B). It suggested that the clays derived from feldspar dissolution blocked the pores and pore throats in the tight sandstone that resulted in a significant decrease in permeability.

As a whole, the porosity and permeability of the studied tight sandstone are controlled by the closed geochemical system during diagenesis. In general, the porosity and permeability increase with the increasing distance to the sandstone/ mudstone interface, especially when the distance is more than 1 m (Figure 12E, F). Therefore, the reservoirs in the tight sandstone of Chang 8 Member mainly develop in the central part of the sandstone. Tight sandstone with thickness more than 2 m could be the potential hydrocarbon reservoirs.

5.6 Implications

As mentioned before, previous studies suggested the reservoir quality of tight sandstone was affected by the diagenesis just based on the descriptions of diagenetic characteristics (Higgs et al., 2007; Lai, Wang, Ran, Zhou, & Cui, 2016; Stroker et al., 2013; Wang et al., 2017; Xi et al., 2015a; Zhou et al., 2016). Although the relationships between diagenesis and reservoir quality have been discussed systematically in most research areas, the essential cause of the tight sandstone reservoir with high porosity remains a puzzle.

Essentially, the origin, transfer, dissolution and precipitation of diagenetic minerals are caused by the water-rock interactions, which were controlled by the diagenetic geochemical system (Bjørlykke & Jahren, 2012). This study discusses the diagenesis which is constrained in the diagenetic geochemical system, and

demonstrates how the precipitation, dissolution and reprecipitation of diagenetic minerals were controlled by the diagenetic geochemical system. Here a combination of the sandstones and adjacent mudstones in Chang 8 Member constitutes a complete and closed system. Although the specific minerals differ, a similar conclusion was concluded by analyzing the diagenesis within the Upper Jurassic Brae Formation of the North Sea, in which solutes were supplied from the mudstones into adjacent sandstones and the average porosity of sandstone displayed a positive correlation with both bed thickness and net to gross (Gluyas, Garland, Oxtoby, & Hogg, 2000).

Due to the relatively closed diagenetic system, the diagenetic fluids could not effectively exchange with the external fluids. Thus, the external sourced carbonate cements mainly develop in the marginal sandstone and could not develop into the central sandstone. In addition, the diagenetic fluids with SiO_2 (aq), Al^{3+} and K^+ are difficult to transfer for a long distance between the mudstone and the adjacent sandstone. As a result, the byproducts of feldspar dissolution including quartz and clay minerals just generate in the central sandstone. The pore space of the central sandstone is preserved and only redistributed. Therefore, the sweet zones in the sandstone reservoirs dominantly develop in the central sandstone. Thus, the reservoir quality of tight oil sandstone is essentially controlled by the diagenetic system. In fact, the diagenetic system can be used for explaining some similar diagenetic characteristics observed in tight sandstone over the world. For example, the carbonate cements commonly concentrated along the sandstone/mudstone interface in Yanchang Formation of Longdong area and Zhenjing area, Ordos Basin and Quantou Formation of southern Songliao Basin, China (Wang et al., 2017; Xi et al., 2015a; Zhou et al., 2016). Moreover, the reaction of feldspar dissolution accompanied with precipitation of authigenic quartz and clays in Quantou Formation of southern Songliao Basin, China and the K3E Kapuni Group in Taranaki Basin, New Zealand (Xi et al., 2015a; Higgs et al., 2007). There is an approximate balance between decrease of primary porosity and increase of secondary porosity in the Upper Cretaceous Mesaverde sandstones of the Piceance Basin, western Colorado (Stroker, et al., 2013). Based on the analysis of this study, it can be concluded that the diagenesis of the above tight

sandstone occurred in a closed diagenetic system. In addition, the dissolution pores developed around the faults in Carboniferous tight sandstone of the Lower Saxony Basin, Northern Germany, suggesting the leaching of acidic fluid in an open diagenetic system (Wüstefeld, Hilse, Koehrer, Adelmann, & Hilgers, 2017). Although detailed clues of diagenetic processes have been given to reveal the intrinsic relation of diagenesis, a comprehensive diagenetic system has been ignored by analyzing diagenesis separately. As a result, the most essential diagenetic process and reservoir heterogeneity of tight sandstone cannot be fully understood. Therefore, the theory of the diagenetic geochemical system should be applied in the study of tight sandstone diagenesis.

That the pattern of diagenetic geochemical system controlling the quality of tight oil sandstone provides a useful analogue for understanding the quality evolution of the tight oil sandstone reservoir which experienced complicated diagenesis. It will be useful for predict the potential reservoirs in other tight sandstones worldwide.

6 CONCLUSIONS

1. The tight sandstone of Chang 8 Member in Xifeng Area are mostly lithic arkoses and feldspathic litharenites with low porosity (mainly 4% to 16%) and permeability (mostly <1mD). And it has undergone significant chemical diagenesis including precipitation of quartz, clay minerals (mainly kaolinite, illite and chlorite) and carbonate (mainly calcite, dolomite, ferrocalcite and ankerite) and dissolution of feldspar.
2. The petrographic textural relationships, the distribution pattern of authigenic minerals and feldspar dissolution, the characteristics of pore water, the salinity of diagenetic fluid and the geologic setting of Xifeng Area, all indicate that the geochemical system was closed during diagenesis period of the tight sandstone reservoir in Chang 8 Member.
3. The relatively closed diagenetic geochemical system impacts the main chemical diagenetic alterations. The carbonate cements preferentially concentrated in the

marginal sandstone (distance to the sandstone/mudstone interface mainly less than 1 m) that result from interaction of the sandstones with carbon (as carbonate) sourced from the adjacent mudstones. The cements of quartz and clay minerals are the byproducts of feldspar dissolution and always associate with feldspar dissolution pores due to internal sources of quartz and clay minerals affected by the closed system.

4. The reservoir quality of the marginal sandstone is poor due to the carbonate cementation, and this effect typically extends no more than 1m from the sandstone margin. Therefore, the reservoirs in the tight sandstone mainly develop in the central part. Tight sandstone with thickness more than 2 m could be the potential hydrocarbon reservoirs.

5. The pattern of diagenetic geochemical system controls the quality of tight oil sandstone, which can provide guidance for predicting the high-quality reservoirs in other tight sandstones worldwide.

ACKNOWLEDGEMENTS

This study was financially supported by the Natural Science Foundation of China (Grant No. 41502147, Grant No. 41672124), Project funded by China Postdoctoral Science Foundation (Grant No. 2016M600752), Sichuan Province Education Department Foundation (Grant No. 16ZA0072) and National science and technology major project of China (2016ZX05047001-002). The PetroChina Research Institute of Petroleum Exploration & Development and PetroChina Changqing Oilfield Company are thanked for providing basic data. Special thanks are extended to the editors and anonymous reviewers for their detailed and constructive suggestions.

REFERENCES

Bjørlykke, K. (1993). Fluid flow in sedimentary basins. *Sedimentary Geology*, *86*, 137-158.

Bjørlykke, K. (1998). Clay mineral diagenesis in sedimentary basins-A key to the

prediction of rock properties. Examples from the North Sea Basin. *Clay Minerals*, *33*, 15-34.

Bjørlykke, K., & Gran. K. (1994). Salinity variations in North Sea formation waters: Implications for large-scale fluid movements. *Marine and Petroleum Geology, 11*, 5-9.

Bjørlykke, K., & Jahren, J. (2012). Open or closed geochemical systems during diagenesis in sedimentary basins: constraints on mass transfer during diagenesis and the prediction of porosity in sandstone and carbonate reservoirs. *AAPG Bulletin, 96*, 2193-2214.

Bodnar, R.J. (1993). Revised equation and table for determining the freezing point depression of H_2O-NaCl solutions. *Geochimica et Cosmochimica Acta, 57*, 683-684.

Boles, J.R., & Franks, S.G. (1979). Clay diagenesis in Wilcox sandstones of southwest Texas: implications of smectite diagenesis on sandstone cementation. *Journal of Sedimentary Research, 49*, 55-70.

Chuhan, F. A., Bjørlykke, K., & Lowrey, C. (2001). Closed system burial diagenesis in reservoir sandstones: Examples from the Garn Formation at Haltenbanken area, offshore mid-Norway. *Journal of Sedimentary Research, 71*, 15-26.

Coplen, T. B., Kendall, C., & Hopple, J. (1983). Comparison of stable isotope reference samples. *Nature, 302*, 236-238.

Cui, Y. F., Wang, G. W., Jones, S. J., Zhou, Z. L., Ran, Y., Lai, J., LI, R. J., & Deng, L. (2017). Prediction of diagenetic facies using well logs -A case study from the upper Triassic Yanchang Formation, Ordos Basin, China. *Marine and Petroleum Geology, 81*, 50-65.

Day-Stirrat, R. J., Milliken, K. L., Dutton, S. P., Loucks, R. G., Hillier, S., Aplin, A. C., & Schleicher, A. M. (2010). Open-system chemical behavior in deep Wilcox Group mudstones, Texas Gulf Coast, USA. *Marine and Petroleum Geology, 27*, 1804-1818.

Dou, W. C., Liu, L. F., Wu, K. J., Xu, Z. J., & Feng, X. (2017). Origin and significance of secondary porosity: A case study of upper Triassic tight

sandstones of Yanchang Formation in Ordos basin, China. *Journal of Petroleum Science and Engineering, 149*, 485-496.

Dutton, S. P., & Loucks, R.G. (2010). Diagenetic controls on evolution of porosity and permeability in lower Tertiary Wilcox sandstones from shallow to ultradeep (200-6700m) burial, Gulf of Mexico Basin, U.S.A. *Marine and Petroleum Geology, 27*, 69-81.

Ehrenberg, S.N. (1990). Relationship between diagenesis and reservoir quality in sandstones of the Garn formation, Haltenbanken, mid-norwegian continental shelf. *AAPG Bulletin, 74*, 1538-1558.

Friedman, I., & O'Neil, J.R. (1977). Compilation of Stable Isotope Fractionation Factors of Geochemical Interest, in Data of Geochemistry. *US Government Printing Office, 440*.

Folk, R.L., 1974. Petrology of Sedimentary Rocks. *Hemphill, 182*.

Fu, J. H., Deng, X. Q., Wang, Q., Li, J.H., Qiu, J. L., Hao, L. W., & Zhao, Y. D. (2017). Densification and hydrocarbon accumulation of Triassic Yanchang Formation Chang 8 Member, Ordos Basin, NW China: Evidence from geochemistry and fluid inclusions. *Petroleum Exploration and Development, 44*, 48-57.

Gier, S., Worden, R. H., Jones, W. D., & Kurzweil, H. (2008). Diagenesis and reservoir quality of Miocene sandstones in the Vienna Basin, Australia. *Marine and Petroleum Geology, 25*, 681-695.

Giles, M.R., & De Boer, R.B. (1990). Origin and significance of redistributional secondary porosity. *Marine and Petroleum Geology, 7*, 378-397.

Gluyas, J., & Coleman, M. L. (1992). Material flux and porosity changes during sediment diagenesis. *Nature, 356*, 52-53.

Gluyas, J.**,** Garland, C., Oxtoby, N. H., & Hogg, A. J. C. (2000). Quartz cement: the Miller's tale. *Quartz cementation in sandstones, 29*,199-218.

Guo, Y. R., Liu, J. B., Yang, H., Liu, Z., Fu, J. H., Yao, J. L., Xu, W. L., & Zhang, Y. L. (2012). Hydrocarbon accumulation mechanism of low permeable tight lithologic oil fields in the Yanchang Formation, Ordos Basin, China. *Petroleum*

Exploration and Development, 39, 447-456.

He, Z. X. (2003). *Evolution and hydrocarbon resource of the Ordos Basin. Petroleum Industry Press. Beijing (in Chinese with English abstract)*.

Higgs, K. E., Zwingmann, H., Reyes, A. G., & Funnell, R. H. (2007). Diagenesis, porosity evolution, and petroleum emplacement in tight gas reservoirs, Taranaki Basin, New Zealand. *Journal of Sedimentary Research, 77*, 1003-1025.

Irwin, H., Curtis, C., & Coleman, M. (1977). Isotopic evidence for source of diagenetic carbonates formed during burial of organic-rich sediments. *Nature, 269*, 209-213.

Law, B. E., & Curtis, J. B. (2002). Introduction to unconventional petroleum systems. *AAPG Bulletin, 86*, 1851-1852.

Lai, J., Wang, G., Ran, Y., Zhou, Z., & Cui, Y. (2016). Impact of diagenesis on the reservoir quality of tight oil sandstones: the case of Upper Triassic Yanchang Formation Chang 7 oil layers in Ordos Basin, China. *Journal of Petroleum Science and Engineering, 145*, 54-65.

Liu, M. J., Liu, Z., Liu, J. J., Zhu, W. Q., Huang, Y. H., & Yao, X. (2014). Coupling relationship between sandstone reservoir densification and hydrocarbon accumulation: A case from the Yanchang Formation of the Xifeng and Ansai areas, Ordos Basin. *Petroleum Exploration and Development, 41*, 185 -192.

Liu, M. J., Liu, Z., Wang, P., & Pan, G. F. (2016). Diagenesis of the Triassic Yanchang Formation Tight Sandstone Reservoir in the Xifeng-Ansai Area of Ordos Basin and its Porosity Evolution. *Acta Geologica Sinica (English Edition), 90*, 956-970.

Liu, M. J., Liu, Z., Wu, Y. W., Zhu, W. Q., & Wang, P. (2017). Differences in formation process of tight sandstone gas reservoirs in different substructures in Changling Fault Depression, Songliao Basin, NE China. *Petroleum Exploration and Development, 44*, 257-264.

Liu, Q. S., Chan, L. S., Liu, Q. S., Li, H. X., Wang, F., Zhang, S. X., Xia, X. H., & Cheng, T. J. (2004). Relationship between magnetic anomalies and hydrocarbon microseepage above the Jingbian gas field, Ordos basin, China. *AAPG Bulletin,*

88, 241-251.

Liu, Z.,Chen, K., Zhu, W. Q., Hu, X. D., Guo, Y. R., & Wu, X. D. (2012). Paleo-pressure restoration of Chang 7 shale in Xifeng area, Ordos Basin. J*ournal of China University Petroleum(Edition of Natural Sciences), 36*, 1-7 (in Chinese with English abstract).

Liu, Z., Zhu, W. Q., Xia, L., Pan, G. F., Wu, X. D., & Guo, Y. R. (2013). Research on oil accumulation process of lithologic reservoir in Chang 8 Member of Yanchang Formation, Xifeng Oilfield. *Geoscience, 27*, 895-906 (in Chinese with English abstract).

Maast, T. E., Jahren, J., & Bjørlykke, K. (2011). Diagenetic controls on reservoir quality in Middle to Upper Jurassic sandstones in the South Viking Graben, North Sea. *AAPG Bulletin*, *95*, 1937 - 1958.

Mansurberg, H., Caja, M. A., Marfil, R., Morad, S., Remacha, E., Martin-Crespo, T., El-Ghali, M.A.K., & Nystuen, J.P. (2009). Diagenetic evolution and porosity destruction of turbiditic hybrid arenites and siliciclastic sandstones of foreland basin: evidence from the Eocene Hecho Group, Pyrenees, Spain. *Journal of Sedimentary Research, 79*, 711-735.

Matthews, A., & Katz, A. (1977). Oxygen isotope fractionation during the dolomitization of calcium carbonate. *Geochimica et Cosmochimica Acta*, *41*, 1431-1438.

Milliken, K.L., & Land, L.S. (1993). The origin and fate of silt sized carbonate in subsurface Miocene-Oligocene mudstones, south Texas Gulf Coast. *Sedimentology, 40*,107-124.

Morad, S., Ketzer, J.M., & DeRos, L.F. (2000). Spatial and temporal distribution of diagenetic alterations in siliciclastic rocks: implications for mass transfer in sedimentary basins. *Sedimentology, 46*, 95-120.

Qiu, X., Liu, C., Wang, F., Deng, Y., & Mao, G. (2015). Trace and rare earth element geochemistry of the upper Triassic mudstones in the southern Ordos Basin, Central China. *Geological Journal, 50*, 399- 413.

Ren, Z.L., Zhang, S., Gao, S.L., Cui, J. P., Xiao, Y. Y., & Xiao, H. (2007). Tectonic

690 thermal history and its significance on the formation of oil and gas accumulation
691 and mineral deposit in Ordos Basin. *Science in China Series D: Earth Sciences, 37*, 23–32.
693 Robinson, A., & Gluyas, J. (1992). Duration of quartz cementation in sandstones, North Sea and Haltenbanken Basins. *Marine and Petroleum Geology, 9*, 324-327.
696 Schmitt, M., Fernandes, C. P., Wolf, F. G., da Cunha Neto, J. A. B., Rahner, C. P., & dos Santos, V. S. S. (2015). Characterization of Brazilian tight gas sandstones relating permeability and Angstrom-to micron-scale pore structures. *Journal of Natural Gas Science and Engineering, 27*, 785-807.
700 Spencer, C. W. (1985). Geologic aspects of tight gas reservoirs in the Rocky Mountain region. *Journal of Petroleum Technology, 37*,1308-1314.
702 Stroker, T.M., Harris, N.B., Crawford Elliott, W., & Marion Wampler, J. (2013). Diagenesis of a tight gas sand reservoir: Upper Cretaceous Mesaverde Group, Piceance Basin, Colorado. *Marine and Petroleum Geology, 40*, 48-68.
705 Taylor, T. R., Giles, M. R., Hathon, L. A., Diggs, T. N., Braunsdorf, N. F., Birbigilia, G. V., Kittridge, M.G., Macaulay, C. I., & Espejo, I. S. (2010). Sandstone diagenesis and reservoir quality prediction: Models, myths, and reality. *AAPG Bulletin, 94*, 1093-1132.
709 Umar, M., Friis, H., Khan, A. S., Kassi, A. M., & Kasi, A. K. (2011). The effects of diagenesis on the reservoir characters in sandstones of the Late Cretaceous Pab Formation, Kirthar Fold Belt, southern Pakistan. *Journal of Asian Earth Sciences, 40*, 622-635.
713 Wang, G. W., Chang, X. C., Yin, W., Li, Y., & Song, T. T. (2017). Impact of diagenesis on reservoir quality and heterogeneity of the Upper Triassic Chang 8 tight oil sandstones in the Zhenjing area, Ordos Basin, China. *Marine and Petroleum Geology, 83*, 84-96.
717 Wu, S. T., Zou, C. N., Zhu, R. K., Yao, J. L., Tao, S. Z., Yang, Z., Zhai, X. F., Cui, J. W., & Lin, S. H. (2016). Characteristics and origin of tight oil accumulations in the Upper Triassic Yanchang Formation of the Ordos Basin, North-Central China.

720 *Acta Geologica Sinica (English Edition), 90*, 1821-1837.
721 Wüstefeld, P., Hilse, U., Koehrer, B., Adelmann, D., & Hilgers, C. (2017). Critical
722 evaluation of an Upper Carboniferous tight gas sandstone reservoir analog:
723 Diagenesis and petrophysical aspects. *Marine and Petroleum Geology, 86*,
724 689-710.
725 Xi, K. L., Cao, Y. C., Jaren, J., Zhu, R. K., Bjørlykke, K., Haile, B. G., Zheng, L. J.,
726 & Hellevang, H. (2015a). Diagenesis and reservoir quality of the Lower
727 Cretaceous Quantou Formation tight sandstones in the southern Songliao Basin,
728 China. *Sedimentary Geology, 330*, 90-107.
729 Xi, K. L., Cao, Y. C., Jaren, J., Zhu, R. K., Bjørlykke, K., Zhang, X. X., Cai, L. X., &
730 Hellevang, H. (2015b). Quartz cement and its origin in tight sandstone reservoirs
731 of the Cretaceous Quantou Formation in the southern Songliao Basin, China.
732 *Marine and Petroleum Geology, 66*, 748-763.
733 Xu, Z. J., Liu, L. F., Wang, T. G., Wu, K. J., Gao, X. Y., Dou, W. C., Xiao, F., Zhang,
734 N. N., Song, X. P., & Ji, H. T. (2017). Application of fluid inclusions to the
735 charging process of the lacustrine tight oil reservoir in the Triassic Yanchang
736 Formation in the Ordos Basin, China. *Journal of Petroleum Science and*
737 *Engineering, 149*, 40-45.
738 Yang, H., Li, S.X., & Liu, X.Y. (2013). Characteristics and resource prospects of tight
739 oil and shale oil in Ordos Basin. *Acta Petrolei Sinica, 34*, 1-11 (in Chinese with
740 English abstract).
741 Yang, H., Liu, X.Y., Zhang, C.L., Han, T.Y., & Hui, X. (2007). The main controlling
742 factors and distribution of low permeability lithologic reservoirs of Triassic
743 Yanchang Formation in Ordos Basin. *Lithologic Reservoirs, 19,* 1-6 (in Chinese
744 with English abstract).
745 Yang, H., & Zhang, W.Z. (2005). Leading effect of the seventh Member high-quality
746 source rock of Yanchang Formation in Ordos Basin during the enrichment of
747 low-penetrating oil-gas accumulation: geology and geochemistry. *Geochimica,*
748 *34*, 147-154 (in Chinese with English abstract).
749 Yang, J. J. (2002). *Tectonic evolution and oil-gas reservoirs distribution in Ordos*

Basin. Petroleum Industry Press. Beijing (in Chinese with English abstract).

Yang, R. C., Jin, Z., J., Van Loon, A., J., Han, Z., Z., & Fan, A., P. (2017). Climatic and tectonic controls of lacustrine hyperpycnite origination in the Late Triassic Ordos Basin, central China: Implications for unconventional petroleum development. *AAPG Bulletin, 101*, 95-117.

Yao, J.L., Deng, X.Q., Zhao, Y.D., Han, T.Y., Chu, M.J., & Pang, X.L. (2013). Characteristics of tight oil in Triassic Yanchang formation, Ordos basin. *Petroleum Exploration and Development, 40*, 161-169.

Yuan, G.H., Cao, Y.C., Gluyas, J., Li, X.Y., Xi, K.L., Wang, Y.Z., Jia, Z.Z., Sun, P.P., & Oxtoby, N.H. (2015b). Feldspar dissolution, authigenic clays, and quartz cements in open and closed sandstone geochemical systems during diagenesis: typical examples from two sags in Bohai Bay Basin, East China. *AAPG Bulletin, 99*, 2121-2154.

Yuan, G.H., Cao, Y.C., Zhang, Y. C., & Gluyas, J. (2017). Diagenesis and reservoir quality of sandstones with ancient “deep” incursion of meteoric freshwaterddAn example in the Nanpu Sag, Bohai Bay Basin, East China. *Marine and Petroleum Geology, 82*, 444-464.

Yuan, G. H., Gluyas, J., Cao, Y. C., Oxtoby, N. H., Jia, Z. Z., Wang, Y. Z., Xi, K. L., & Li, X. Y. (2015a). Diagenesis and reservoir quality evolution of the Eocene sandstones in the northern Dongying Sag, Bohai Bay Basin, East China. *Marine and Petroleum Geology, 62*, 77-89.

Zhang, W.Z., Yang, H., Li, J. F., & Ma, J. (2006). Leading effect of high class source rock of Chang 7 in Ordos Basin on enrichment of low permeability oil-gas accumulation: Hydrocarbon generation and expulsion mechanism. *Petroleum Exploration and Development, 33*, 289-293 (in Chinese with English abstract).

Zhang, W.Z., Yang, H., Hou, L.H., & Liu, F. (2009). Distribution and geological significance of 17α (H)-diahopanes from different hydrocarbon source rocks of Yanchang Formation in Ordos Basin. *Science in China Series D: Earth Sciences, 52*, 965-974.

Zhang, Y., Pe-piper, G., & Piper, D. J.W. (2015). How sandstone porosity and

780 permeability vary with diagenetic minerals in the Scotian Basin, offshore eastern
781 Canada: Implications for reservoir quality. *Marine and Petroleum Geology, 63*,
782 28-45.
783 Zhang, Y. L., Bao, Z. D., Zhao, Y., Jiang, L., & Gong, F. H. (2017). Diagenesis and its
784 controls on reservoir properties and hydrocarbon potential in tight sandstone: a
785 case study from the Upper Triassic Chang 7 oil group of Yanchang Formation,
786 Ordos Basin, China. *Arabian Journal of Geosciences*, *10*, 234.
787 Zhou, Y., Ji, Y. L., Xu, L. M., Che, S. Q., Niu, X. B., Wan, L., Zhou, Y. Q., Li, Z. C.,
788 & You, Y. (2016). Controls on reservoir heterogeneity of tight sand oil reservoirs
789 in Upper Triassic Yanchang Formation in Longdong Area, southwest Ordos
790 Basin, China: Implications for reservoir quality prediction and oil accumulation.
791 *Marine and Petroleum Geology, 78*, 110-135.
792 Zhu, H. H., Zhong, D.K., Yao, J.L., Sun, H.T., Niu, X.B., Liang, X.W., You, Y., & Li,
793 X. (2015).
794 Alkaline diagenesis and its effects on reservoir porosity: a case study of Upper
795 Triassic Chang7 Member tight sandstone in Ordos Basin, NW China. *Petroleum*
796 *Exploration and Development, 42*, 56-65.
797 Zou, C. N., Wang, L., Li, Y., Tao, S. Z., & Hou, L. H. (2012b). Deep-lacustrine
798 transformation of sandy debrites into turbidites, Upper Triassic, Central China.
799 *Sedimentary Geology, 265*, 143-155.
800 Zou, C.N., Zhang, G.Y., Tao, S.Z., Hu, S.Y., Li, X.D., Li, J.Z., Dong, D.Z., Zhu, R.K.,
801 Yuan, X.J., Hou, L.H., Qu, H., Zhao, X., Jia, J.H., Gao, X.H., Guo, Q.L., Wang,
802 L., & Li, X.J. (2010a). Geological features, major discoveries and
803 unconventional petroleum geology in the global petroleum exploration.
804 *Petroleum Exploration and Development, 37*, 129-145.
805 Zou, C.N., Zhang, X. Y., Luo, P., Wang, L., Luo, Z., & Liu, L. H. (2010b).
806 Shallow-lacustrine sand-rich deltaic depositional cycles and sequence
807 stratigraphy of the Upper Triassic Yanchang Formation, Ordos Basin, China.
808 *Basin Research*, *22*, 108-125.
809 Zou, C.N., Zhu, R.K., Liu, K., Su, L., Bai, B., & Zhang, X. (2012a). Tight gas

sandstone reservoirs in China: characteristics and recognition criteria. *Journal of Petroleum Science and Engineering, 88*, 82-91.

Table 1

Mineralogical and isotopic composition of carbonate cements, and calculated formation temperature of cements in Chang 8 member tight sandstones of Xifeng Area. Ca-calcite, Do-dolomite, Fc-ferrocalcite, An-ankerite

Well	Depth, m	Carbonate mineral	$\delta^{13}C_{PDB}$ ‰	$\delta^{18}O_{PDB}$ ‰	Temper-ature,℃ $\delta^{18}O_{SMOW}$ =-7‰	Well	Depth, m	Carbonate mineral	$\delta^{13}C_{PDB}$ ‰	$\delta^{18}O_{PDB}$ ‰	Temper-ature,℃ $\delta^{18}O_{SMOW}$=-7‰
Wu121	2070.3	100%An	-2.18	-18.47	103.70	Xi200	2202.5	100%An	-5.35	-18.72	105.95
Wu121	2083.5	75%An+15%Ca+10% Do	-3.48	-20.10	118.88	Xi203	1873.6	100%An	-3.69	-18.71	105.83
Wu121	2076.8	100%An	-6.42	-20.12	119.00	Xi211	1580.5	100%An	-6.49	-17.59	96.28
Wu121	2081.55	100%Fc	-1.39	-17.36	79.93	Xi211	1548.1	95%Ca+5%Do	1.00	-12.88	49.03
Wu121	2082.45	90%Fc+10%An	-6.14	-19.32	96.53	Xi220	1944.9	100%An	-3.98	-19.87	116.65
Wu121	2093.9	100%Fc	-3.32	-20.15	104.30	Xi23	2095	100%An	-7.44	-16.75	89.51
Wu121	2090.5	100%Fc	-5.68	-19.98	102.68	Xi23	2090.7	100%An	-5.58	-18.04	100.05
Wu121	2087.9	100%Fc	-2.21	-19.59	98.98	Xi32	1940	100%An	-4.48	-19.50	113.11
Wu121	2081	90%Do+10%Ca	-0.67	-10.89	51.02	Xi33	1996.5	100%An	-5.19	-20.39	121.73
Wu64	2067.4	100%An	-5.50	-17.39	94.64	Xi34	1993.2	100%An	-4.00	-19.22	110.45
Wu64	2068.35	60%An+40%Ca	-4.77	-17.79	97.94	Xi53	2013	100%An	-3.98	-19.82	116.12
Wu64	2084.7	100%An	-0.66	-19.12	109.55	Xi53	2012	100%An	-4.82	-20.09	118.73
Wu64	2074.5	100%An	-6.52	-19.41	112.22	Xi55	2017.4	95%Ca+5%Fc	-9.63	-16.62	74.17
Wu64	2086.2	100%An	-5.68	-19.66	114.63	Xi58	2135.5	100%An	-6.21	-18.59	104.79
Wu64	2089.8	100%An	-4.06	-20.02	118.06	Zhen383	2279	70%An+25%Ca +5%Do	-7.68	-17.34	94.25
Wu64	2078.8	100%An	-5.66	-20.05	118.35	Zhen383	2272.2	95%An+5%Ca	-6.72	-19.42	112.31
Wu64	2081.7	40%An+30%Ca+30% Do	-5.41	-20.36	121.42	Zhen383	2305.95	95%An+5%Ca	-1.34	-20.72	125.09
Wu64	2084.1	95%An+5%Ca	-2.34	-20.39	121.74	Zhen383	2302.8	95%An+5%Ca	-6.61	-20.74	125.31
Wu64	2072	100%An	-8.12	-20.69	124.79	Zhen383	2283.47	95%An+5%Do	-5.12	-20.77	125.63
Wu64	2070.5	95%An+5%Do	-8.21	-20.91	127.11	Zhen383	2303.85	80%An+15%Ca +5%Do	-2.58	-21.18	129.95
Wu64	2079.7	60%An+40%Do	-9.85	-21.04	128.41	Zhen383	2300	100%An	-2.80	-21.40	132.32
Wu64	2081.2	90%An+10%Fc	-7.40	-21.50	133.38	Zhen383	2272.35	85%Fc+15%An	-4.11	-19.16	95.11
Wu64	2091.3	40%An+30%Ca+30% Do	-2.96	-22.11	140.32	Zhen383	2278.6	100%Fc	-6.14	-20.13	104.07
Wu64	2073.4	60%Fc+40%An	-5.19	-20.18	104.58	Zhen383	2280.42	95%Fc+5%An	-0.80	-20.75	110.20
Wu64	2089.1	75%Fc+25%An	-4.88	-20.20	104.74	Zhen383	2299.5	100%Fc	-6.32	-21.23	115.18
Wu64	2076.3	100%Fc	-5.04	-19.59	99.03	Zhen383	2278	90%Ca+10%Do	-10.23	-16.35	72.14
Xi128	1987.55	100%An	-5.05	-19.47	112.79	Zhen383	2302.36	95%Ca+5%An	-6.66	-20.78	110.57
Xi128	1986.45	100%An	-7.77	-20.84	126.38	Zhen383	2285.15	80%Do+15%Ca +5%Fc	-9.62	-13.14	64.29
Xi17	2148.4	100%Fc	-4.20	-20.58	108.48	Zhuang20	1848	100%An	-6.08	-19.78	115.77
Xi180	2112.1	100%Fc	-5.08	-19.61	99.16						

Note: The formula used in calculating calcite mineral temperature is $1000\ln\alpha_{calcite\text{-}water} = 2.78 \times 10^6/T^2\text{-}2.89$ (Friedman and O'Neil, 1977); the formula used in calculating dolomite mineral temperature is $1000\ln\alpha_{dolomite\text{-}water}=3.06\times10^6/T^2\text{-}3.24$ (Matthews and Katz, 1977); $1000\ln\alpha_{carbonate\text{-}water}= \delta^{18}O_{carbonate}–\delta^{18}O_{water}$; and $\delta^{18}O_{SMOW}$ (‰) $=1.03091\delta^{18}O_{PDB}+30.91$(Coplen, et al., 1983).

Table 2

Microthermometric data of the aqueous fluid inclusions in Chang 8 member tight sandstone reservoirs.

Well	Depth, m	Host mineral	Size, μm	types	Th, ℃	Tm, ice/℃	Salinity, NaCl wt.% equiv.(from Bodnar,1993)	Well	Depth,m	Host mineral	Size, μm	types	Th, ℃	Tm, ice/℃	Salinity, NaCl wt.% equiv.(from Bodnar,1993)
Wu121	2087.9	Carbonate cement	3×8	Aqueous	56.4	-4.8	7.59	Xi23	2095	Carbonate cement	2×4	Aqueous	68.3	-2.9	4.80
Wu121	2087.9	Carbonate cement	2×2	Aqueous	68.5	-4.3	6.88	Xi23	2095	Carbonate cement	2×2	Aqueous	54.8	-2.6	4.34
Wu121	2087.9	Quartz overgrowth	2×2	Aqueous	104.3	-5.1	8.00	Xi23	2095	Quartz overgrowth	4×7	Aqueous	106	-4.6	7.31
Wu64	2081.2	Carbonate cement	2×10	Aqueous	54.2	-4.7	7.45	Xi23	2095	Carbonate cement	2×3	Aqueous	81.6	-2.5	4.18
Wu64	2081.2	Carbonate cement	2×4	Aqueous	63.9	-4.9	7.73	Xi23	2095	Quartz overgrowth	3×5	Aqueous	112	-14.5	18.22
Wu64	2081.2	Quartz overgrowth	2×2	Aqueous	99.7	-5.2	8.14	Xi23	2095	Quartz overgrowth	5×9	Aqueous	119	-5.6	8.68
Wu64	2081.2	Quartz overgrowth	2×5	Aqueous	102.8	-4.5	7.17	Xi23	2095	Quartz overgrowth	2×5	Aqueous	120	-10.7	14.67
Xi128	1987.55	Quartz overgrowth	2×3	Aqueous	88.6	-4.2	6.74	Xi32	1940	Quartz overgrowth	3×6	Aqueous	85.9	-3.9	6.30
Xi128	1987.55	Quartz overgrowth	2×6	Aqueous	95.8	-4.3	6.88	Xi32	1940	Quartz overgrowth	2×2	Aqueous	86.5	-4.2	6.74
Xi17	2148.4	Authigenic quartz	3×5	Aqueous	71	-12.9	16.80	Xi32	1940	Quartz overgrowth	3×3	Aqueous	89.3	-4.6	7.31
Xi17	2148.4	Quartz overgrowth	2×12	Aqueous	77.3	-13.1	16.99	Xi33	1996.5	Quartz overgrowth	3×5	Aqueous	96.5	-9.1	12.96
Xi17	2148.4	Quartz overgrowth	5×6	Aqueous	82.5	-14.5	18.22	Xi33	1996.5	Quartz overgrowth	2×2	Aqueous	98.4	-4.1	6.59
Xi17	2148.4	Authigenic	3×10	Aqueous	90	-8.9	12.73	Xi33	1996.5	Carbonate	2×4	Aqueous	51.7	-3.4	5.56

		quartz								cement				
Xi17	2148.4	Carbonate cement	2×2	Aqueous	68.5	-10.9	14.87	Xi34	1993.2	Carbonate cement	2×6	Aqueous	63.4	-16.2	19.60
Xi17	2148.4	Quartz overgrowth	2×3	Aqueous	121	-11.5	15.47	Xi34	1993.2	Carbonate cement	2×5	Aqueous	68.6	-15.4	18.96
Xi180	2112.1	Quartz overgrowth	3×6	Aqueous	79.2	-5.3	8.28	Xi53	2013	Quartz overgrowth	2×4	Aqueous	120.4	-12.1	16.05
Xi180	2112.1	Quartz overgrowth	2×5	Aqueous	80.7	-7.9	11.58	Xi55	2017.4	Quartz overgrowth	3×4	Aqueous	93.5	-8.4	12.16
Xi180	2112.1	Quartz overgrowth	3×5	Aqueous	83.7	-9.2	13.07	Xi55	2017.4	Carbonate cement	2×6	Aqueous	63.3	-8.9	12.73
Xi180	2112.1	Quartz overgrowth	3×5	Aqueous	108.5	-8.7	12.51	Xi55	2017.4	Quartz overgrowth	3×8	Aqueous	97.6	-9.3	13.18
Xi180	2112.1	Quartz overgrowth	2×3	Aqueous	121.8	-17.6	20.67	Xi58	2135.5	Carbonate cement	2×2	Aqueous	66.2	-8.2	11.93
Xi200	2202.5	Carbonate cement	2×6	Aqueous	62.8	-16.3	19.68	Xi58	2135.5	Quartz overgrowth	2×5	Aqueous	97.9	-9.5	13.40
Xi200	2202.5	Carbonate cement	2×8	Aqueous	64.6	-16.9	20.15	Xi58	2135.5	Quartz overgrowth	3×3	Aqueous	101.5	-4.8	7.59
Xi200	2202.5	Carbonate cement	2×8	Aqueous	106.5	-15.1	18.72	Zhen383	2302.36	Carbonate cement	3×10	Aqueous	54.2	-16.8	20.07
Xi200	2202.5	Carbonate cement	2×6	Aqueous	108.4	-15.8	19.29	Zhen383	2302.36	Carbonate cement	2×6	Aqueous	109.3	-15.7	19.21
Xi200	2202.5	Carbonate cement	2×10	Aqueous	109.1	-15.5	19.05	Zhen383	2302.36	Carbonate cement	3×4	Aqueous	114.6	-15.5	19.05
Xi203	1873.6	Carbonate cement	2×2	Aqueous	56.7	-9.4	13.29	Zhen383	2302.36	Carbonate cement	3×8	Aqueous	117.8	-16.3	19.68
Xi211	1780.5	Quartz overgrowth	2×3	Aqueous	92.4	-3.9	6.30	Zhuang20	1848	Quartz overgrowth	2×2	Aqueous	90.3	-8.4	12.16
Xi211	1780.5	Quartz overgrowth	2×5	Aqueous	94.1	-3.6	5.86	Zhuang20	1848	Quartz overgrowth	3×10	Aqueous	93.2	-7.9	11.58

Xi220	1943.7	Quartz overgrowth	2×4	Aqueous	85.9	-2.1	3.55	Zhuang20	1848	Carbonate cement	3×5	Aqueous	65.7	-8.1	11.81
Xi220	1943.7	Quartz overgrowth	2×7	Aqueous	86.7	-2.9	4.80	Zhuang20	1848	Carbonate cement	2×6	Aqueous	66.4	-8.8	12.62
Xi220	1943.7	Quartz overgrowth	2×2	Aqueous	88.2	-2.6	4.34	Zhuang52	1953.5	Quartz overgrowth	2×3	Aqueous	117.8	-6.7	10.11
Xi220	1943.7	Carbonate cement	3×5	Aqueous	64.8	-2.5	4.18	Zhuang52	1953.5	Quartz overgrowth	2×5	Aqueous	123.5	-16.9	20.15
Xi23	2095	Carbonate cement	2×5	Aqueous	55.5	-2.3	3.87	Zhuang53	2013	Quartz overgrowth	2×4	Aqueous	96.7	-10.1	14.04

Note: The formula used in calculating salinity is $S=0.00+1.78T-0.0442T^2+0.000557T^3$ (Bodnar, 1993); T_h-homogenization temperature; T_m-final ice melting temperature

Figure captions

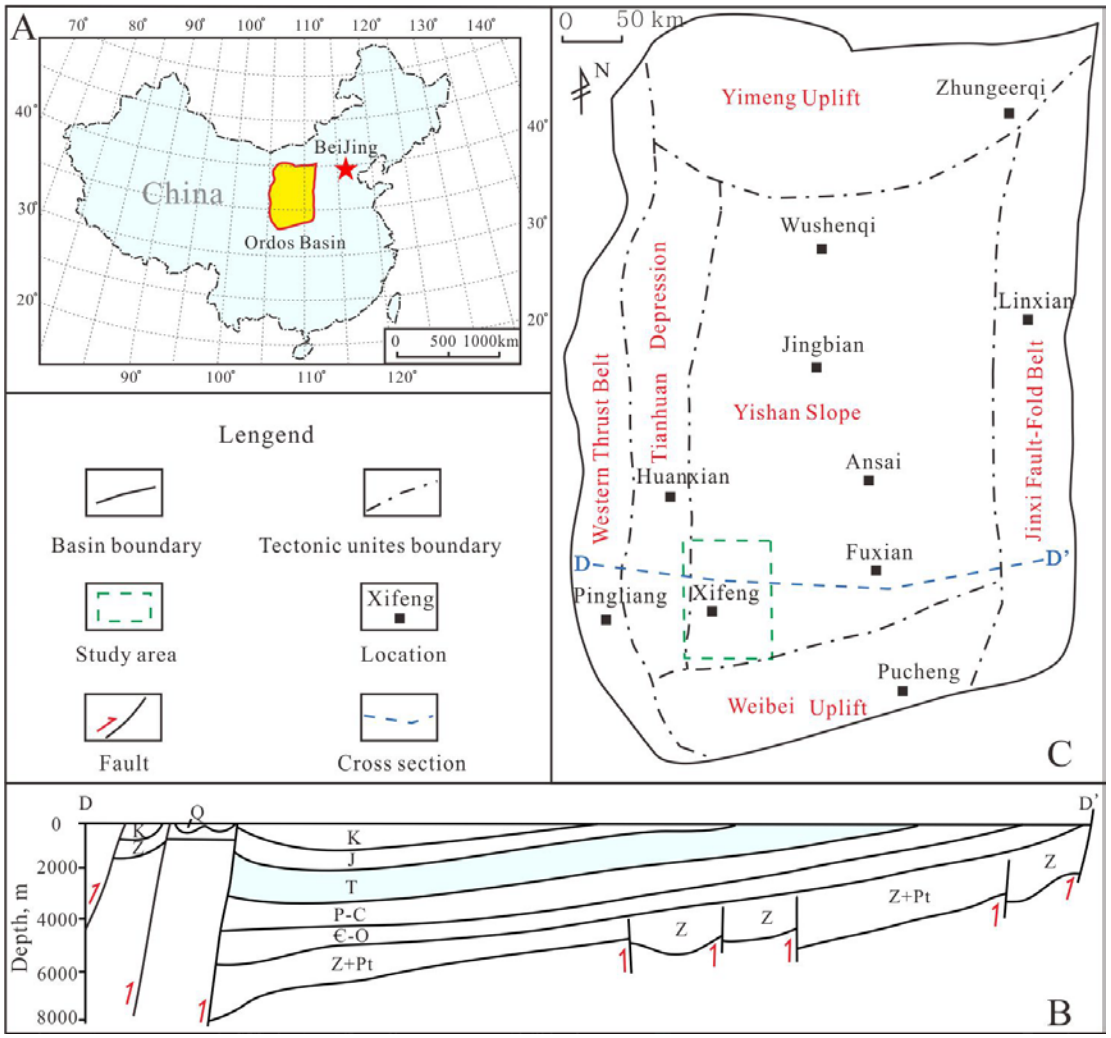

Figure 1. (A) Location map of the Ordos Basin, China. (B) Cross-section (DD' in Figure 1C) of the Ordos Basin showing the various tectonic units and strata (Triassic rocks in blue). (C) Simplified tectonic units and location map of the Xifeng Area in the Ordos Basin (modified from Liu et al., 2016).

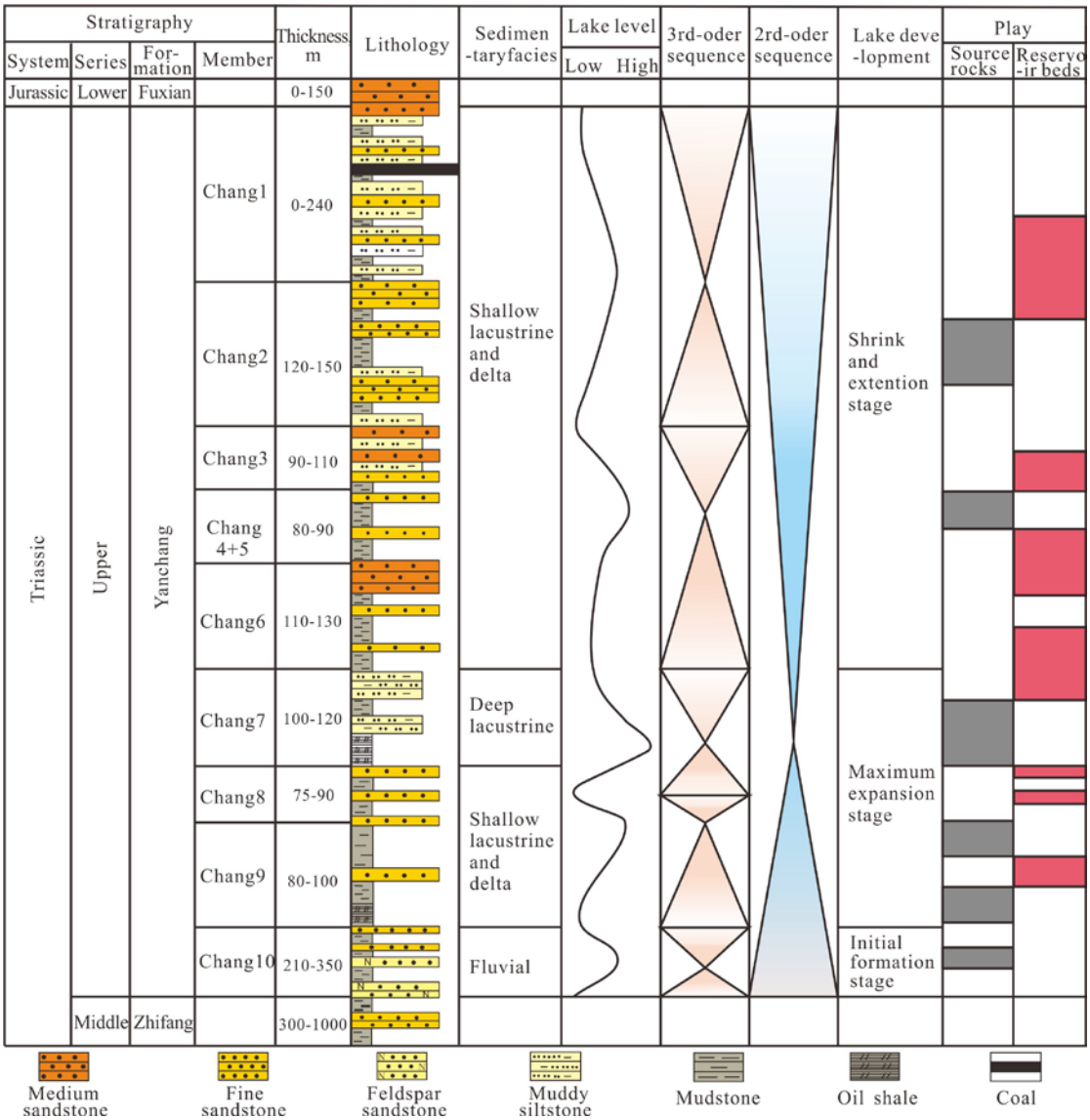

Figure 2. The composite stratigraphic columns of the Yanchang Formation in Ordos Basin, showing the evolutions of lake level, lake development and sedimentary facies and the major elements of tight sandstone hydrocarbon reservoir (modified from Zhou et al., 2016 and Xu et al., 2017).

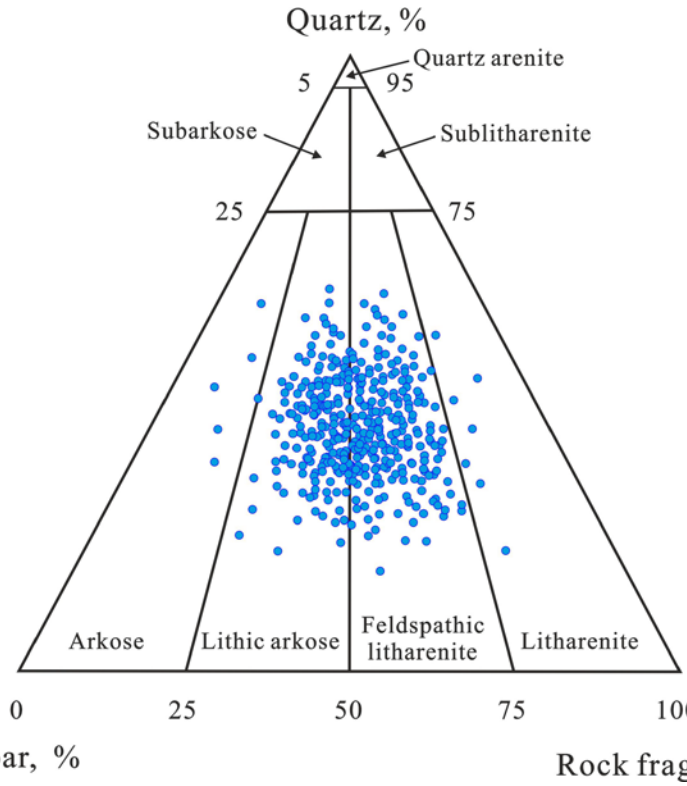

Figure 3. Rock composition of the Chang 8 Member tight sandstone of Yanchang Formation in the Xifeng Area plotted on Folk's (1974) ternary diagram.

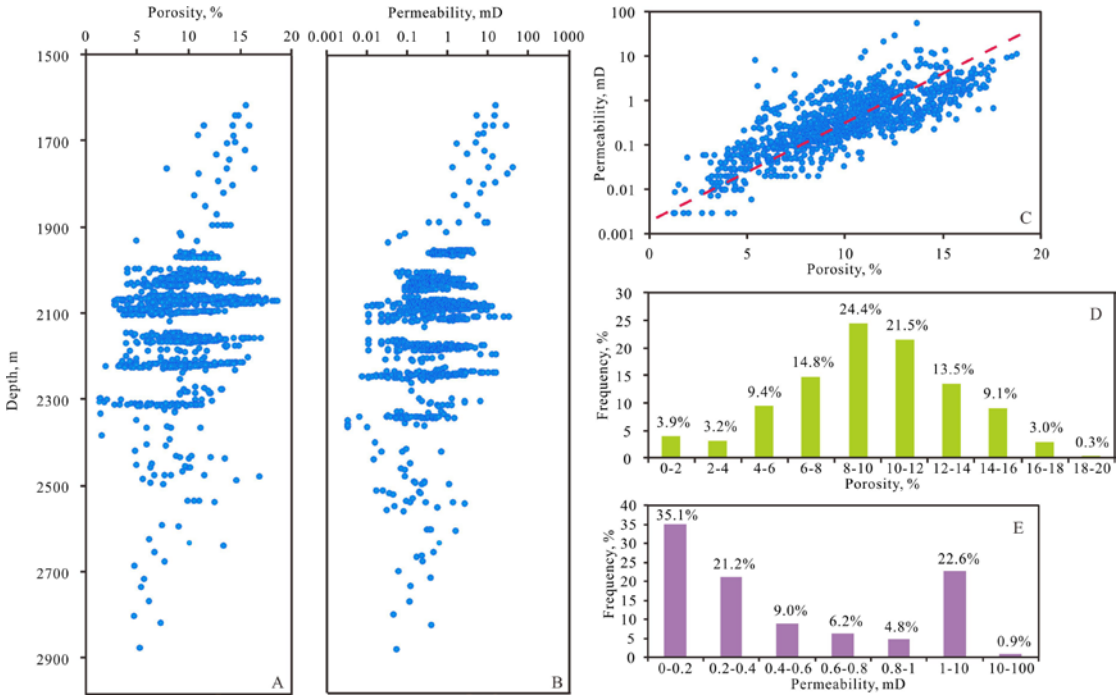

Figure 4. Characteristics of Chang 8 Member tight sandstone reservoir properties in Xifeng Area: (A) Porosity versus depth. (B) Permeability versus depth. (C) Porosity versus permeability. (D) Porosity distribution. (E) Permeability distribution.

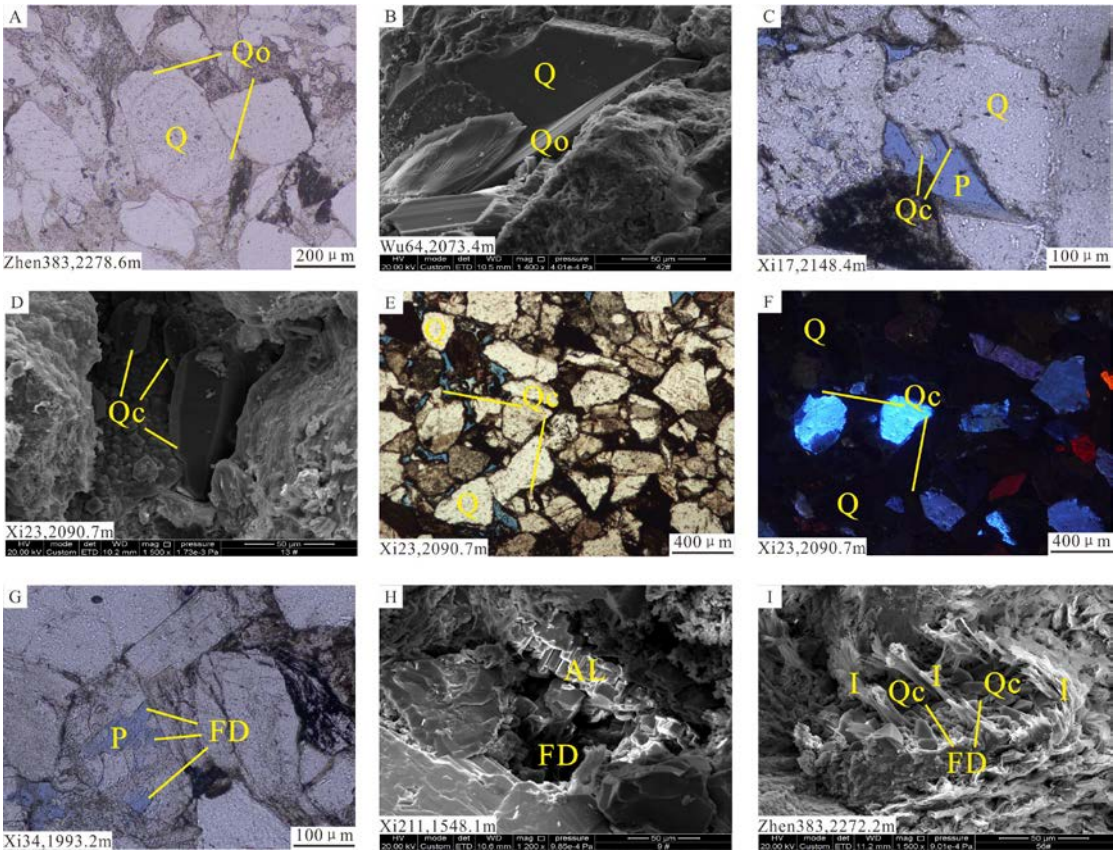

Figure 5. Characteristics of quartz cements and feldspar dissolution in Chang 8 Member tight sandstone reservoirs (pore space is shown in blue). (A) Micrograph of thin section showing the quartz overgrowth. (B) Micrograph of SEM showing the quartz overgrowth. (C) Micrograph of thin section showing the authigenic quartz crystal. (D) Micrograph of SEM showing the authigenic quartz crystal. (E) Micrograph of thin section showing the authigenic quartz crystal. (F) Idem with E but micrograph of CL. (G) Micrograph of thin section showing feldspar partly dissolved. (H) Micrograph of SEM showing feldspar dissolution and authigenic albite. (H) Micrograph of SEM showing feldspar dissolution, authigenic quartz crystal and authigenic fibrous illite. Q-Quartz detrital grain; Qo-Quartz overgrowth; Qc-Quartz crystal; P- Pores; FD-Feldspar dissolution; AL-Albite; I-Illite.

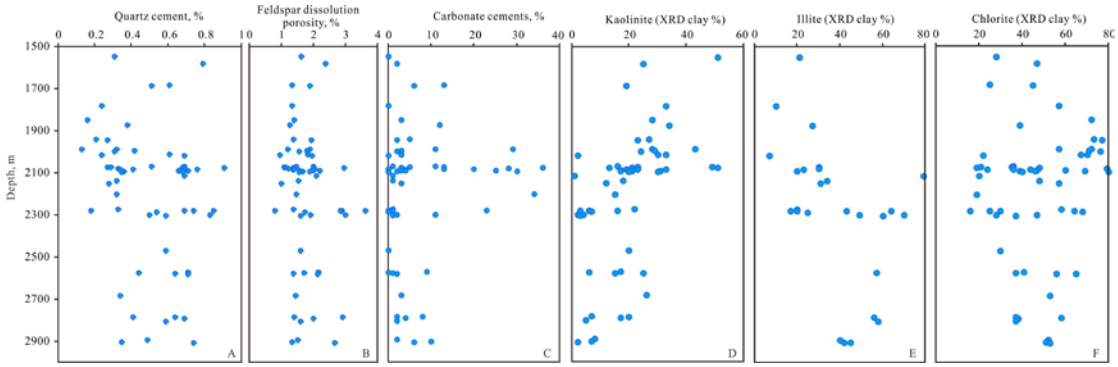

Figure 6. Vertical distribution characteristics of quartz cement (A), feldspar dissolution porosity (B), carbonate cements (C), kaolinite (D), illite (E) and chlorite (F) in Chang 8 Member tight sandstone reservoirs, Xifeng Area.

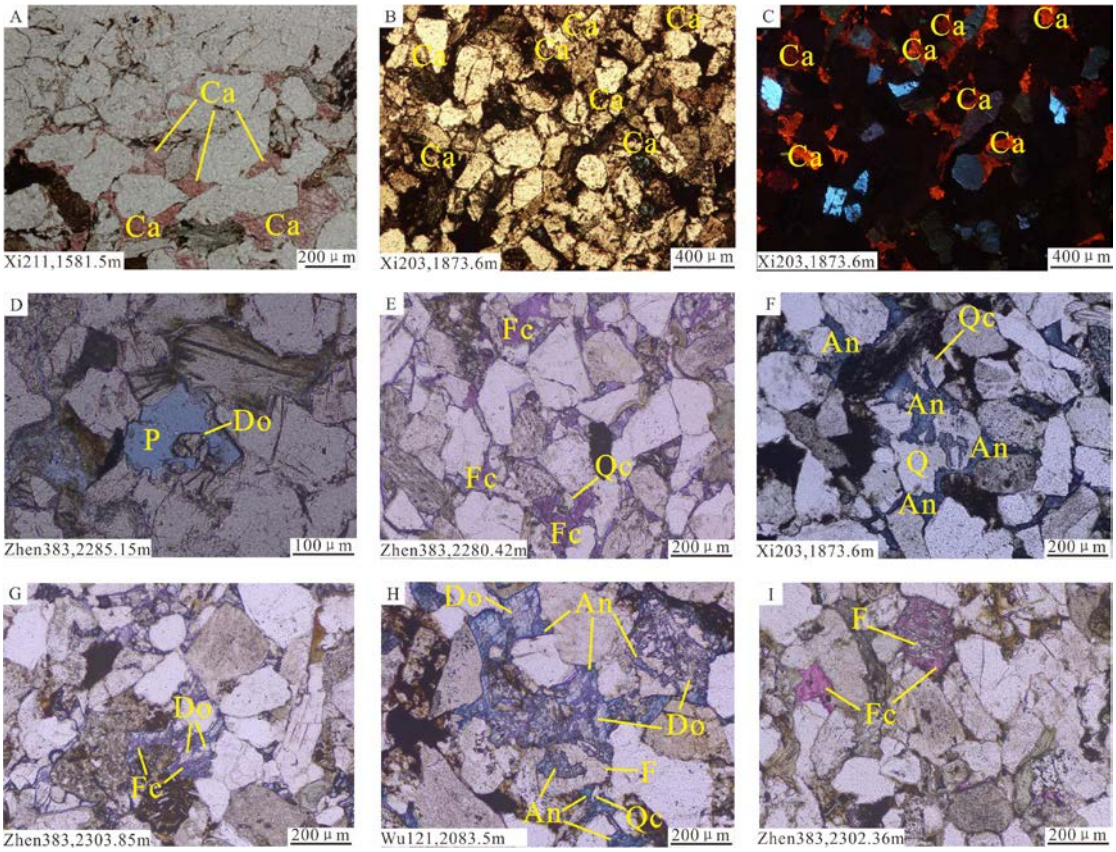

Figure 7. Characteristics of carbonate cements in Chang 8 Member tight sandstone reservoirs. (A) Micrograph of thin section showing the pore-filling calcite cement. (B) Micrograph of thin section showing the pore-filling calcite cement. (C) Idem with B but micrograph of CL. (D) Micrograph of thin section showing the euhedral rhombs of dolomite cement partly filling the intergranular pore. (E) Micrograph of thin section showing the ferrocalcite cements around the euhedral quartz crystal. (F) Micrograph of thin section showing the ankerite cements around the euhedral quartz crystal and partly replacing quartz grain. (G) Micrograph of thin section showing the ferrocalcite cements partly replacing dolomite cements. (H) Micrograph of thin section showing the ankerite cements partly replacing dolomite cements and completely filling feldspar dissolution pore. (I) Micrograph of thin section showing the ferrocalcite cements completely filling feldspar dissolution pore. Q-Quartz detrital grain; Qc-Quartz crystal; P- Pores; F-Feldspar; Ca-Calcite; Do-Dolomite; Fc-Ferrocalcite; An-Ankerite.

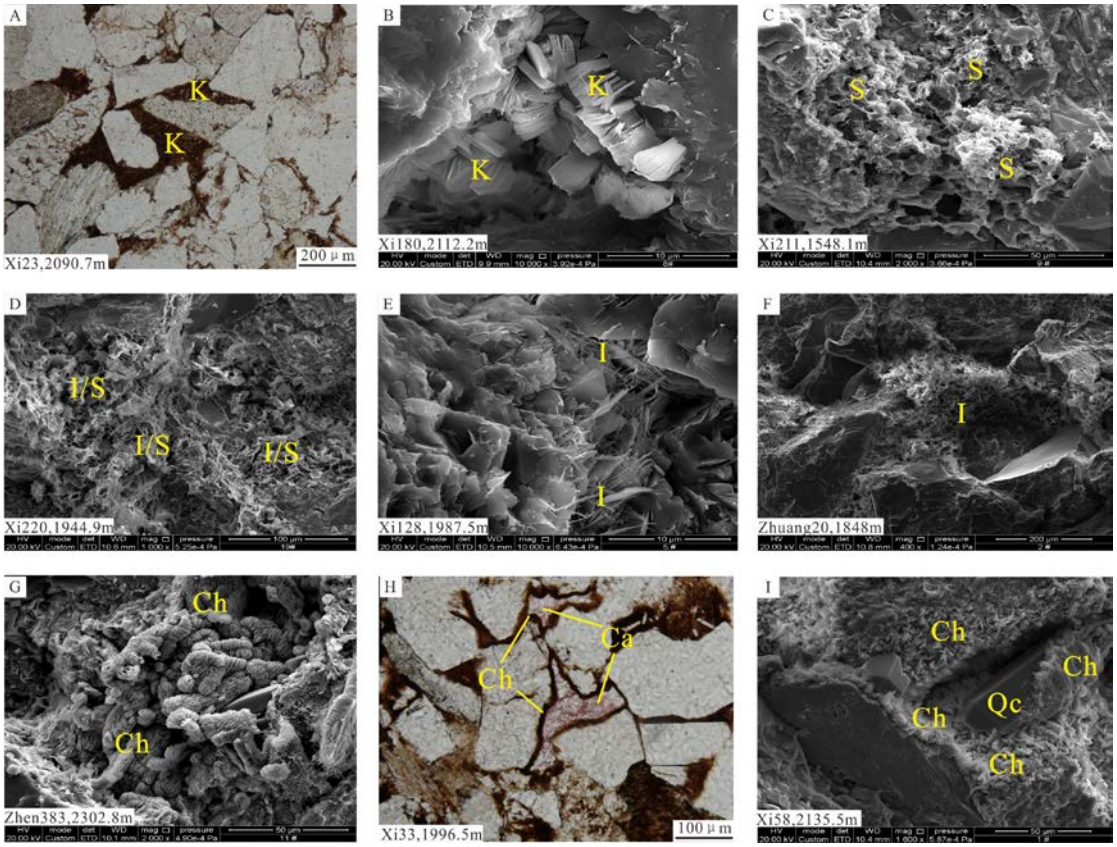

Figure 8. Characteristics of clay cements in Chang 8 Member tight sandstone reservoirs. (A) Micrograph of thin section showing pore-filling kaolinite. (B) Micrograph of SEM showing authigenic vermicular kaolinite. (C) Micrograph of SEM showing authigenic curly flaky smectite. (D) Micrograph of SEM showing authigenic honeycomb I/S. (E) Micrograph of SEM showing authigenic fibrous illite. (F) Micrograph of SEM showing authigenic honeycomb illite. (G) Micrograph of SEM showing authigenic rosette-shaped chlorite. (H) Micrograph of thin section showing authigenic chlorite rim covering detrital grain. (I) Micrograph of SEM showing authigenic needle chlorite coating covering authigenic quartz crystal. Ca-Calcite; Qc-Quartz crystal; K-Kaolinite; S-Smectite; I/S-mixed-layer illite/smectite; I-Illite; Ch-Chlorite.

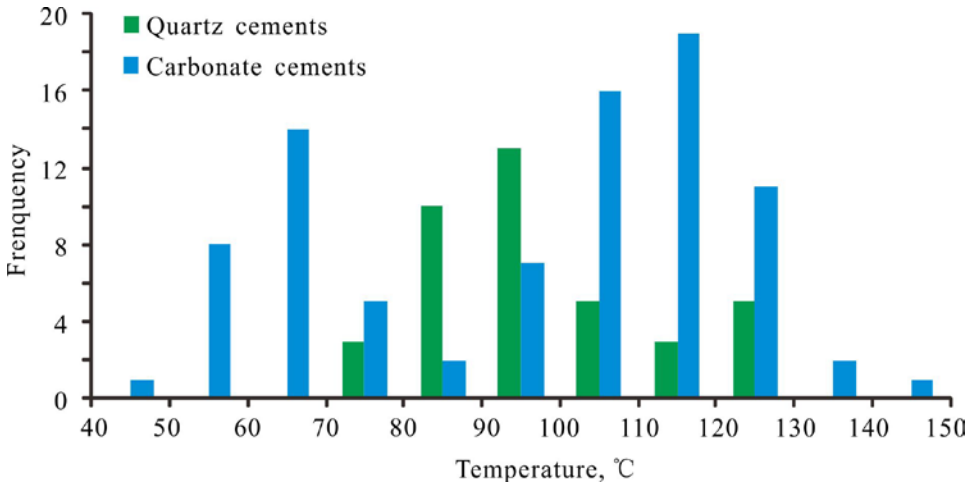

Figure 9. Comparison of the homogenization temperatures of the aqueous inclusions in quartz cements and carbonate cements (including the approximate carbonate cements precipitation temperatures are calculated by oxygen isotope) in Chang 8 Member tight sandstone reservoirs.

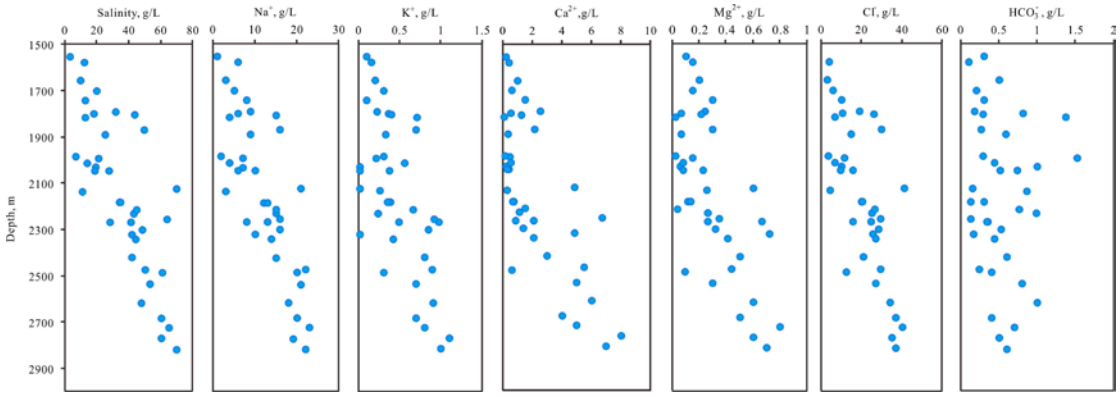

Figure 10. Salinity and concentration of different ions in pore water from Chang 8 Member tight sandstone in Xifeng Area.

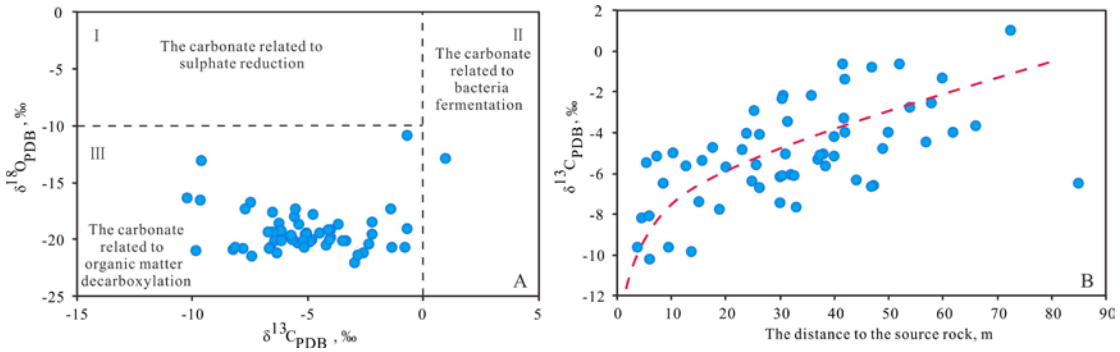

Figure 11. The distribution characteristics of isotopes. (A) Introduction of carbonate and oxygen isotope distribution (modified from Irwin et al., 1977; Xi et al., 2015a). (B) $\delta^{13}C$ values increase with the increasing distance of samples to source rocks.

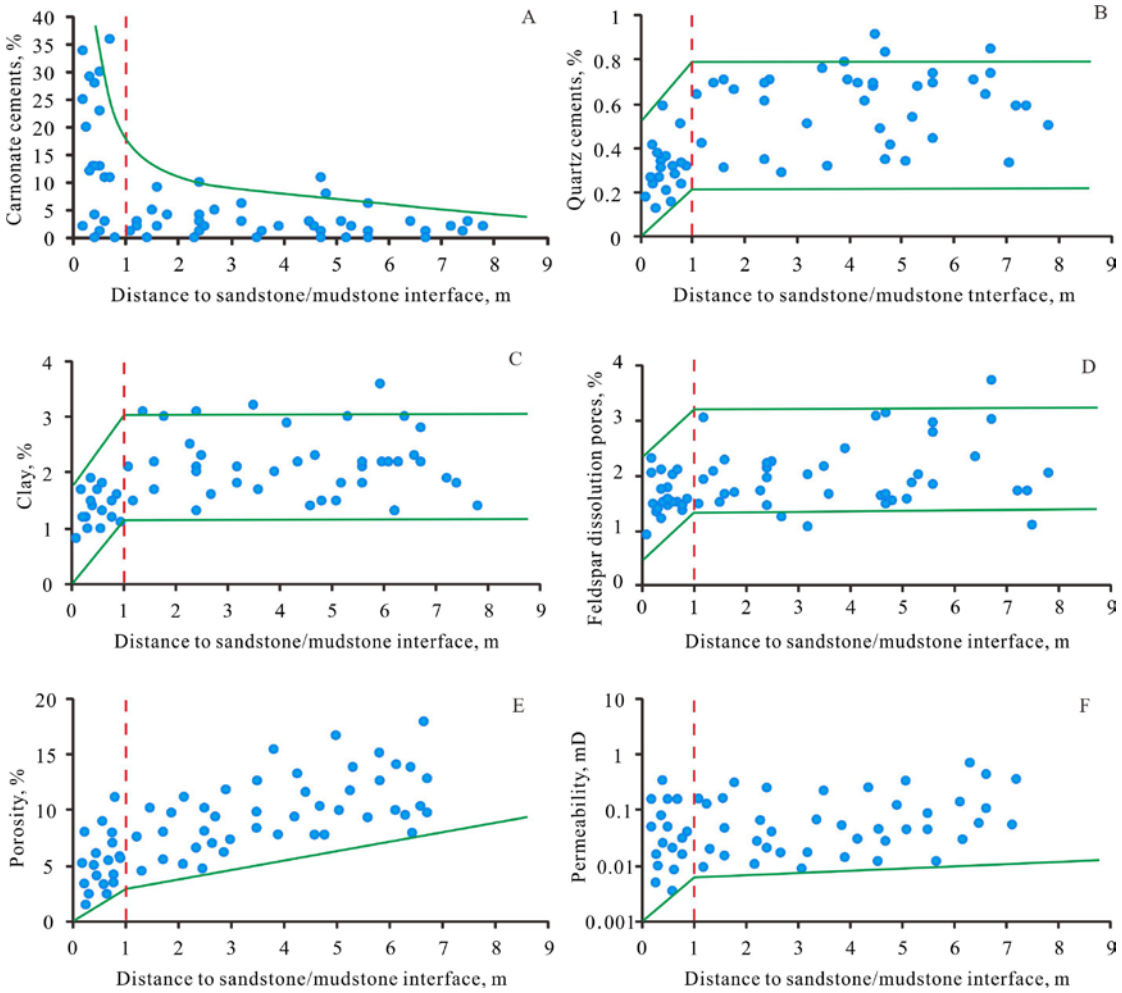

Figure 12. Relationship between sandstone reservoir quality and the distance to sandstone/mudstone interface. (A) Cross-plot between the content of carbonate cements and the distance to sandstone/mudstone interface. (B) Cross-plot between the content of quartz cements and the distance to sandstone/mudstone interface. (C) Cross-plot between the content of clay minerals and the distance to sandstone/mudstone interface. (D) Cross-plot between the feldspar dissolution pores and the distance to sandstone/mudstone interface. (E) Cross-plot between the porosity and the distance to sandstone/mudstone interface. (F) Cross-plot between the permeability and the distance to sandstone/mudstone interface.

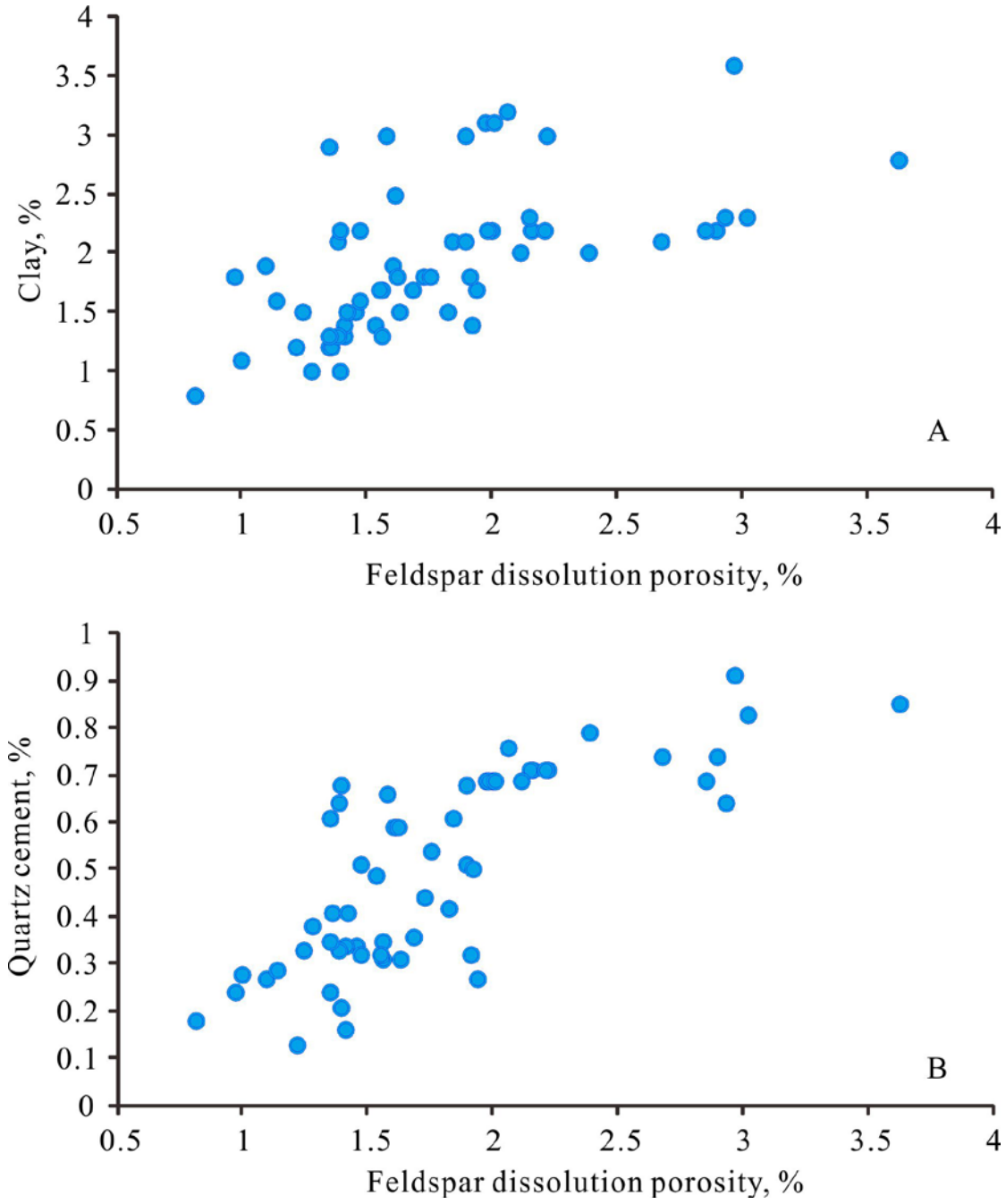

933

934 **Figure 13.** Relationship between the content of feldspar dissolution porosity,
935 authigenic clay (A) and quartz cement (B) in Chang 8 Member tight sandstone in
936 Xifeng Area.

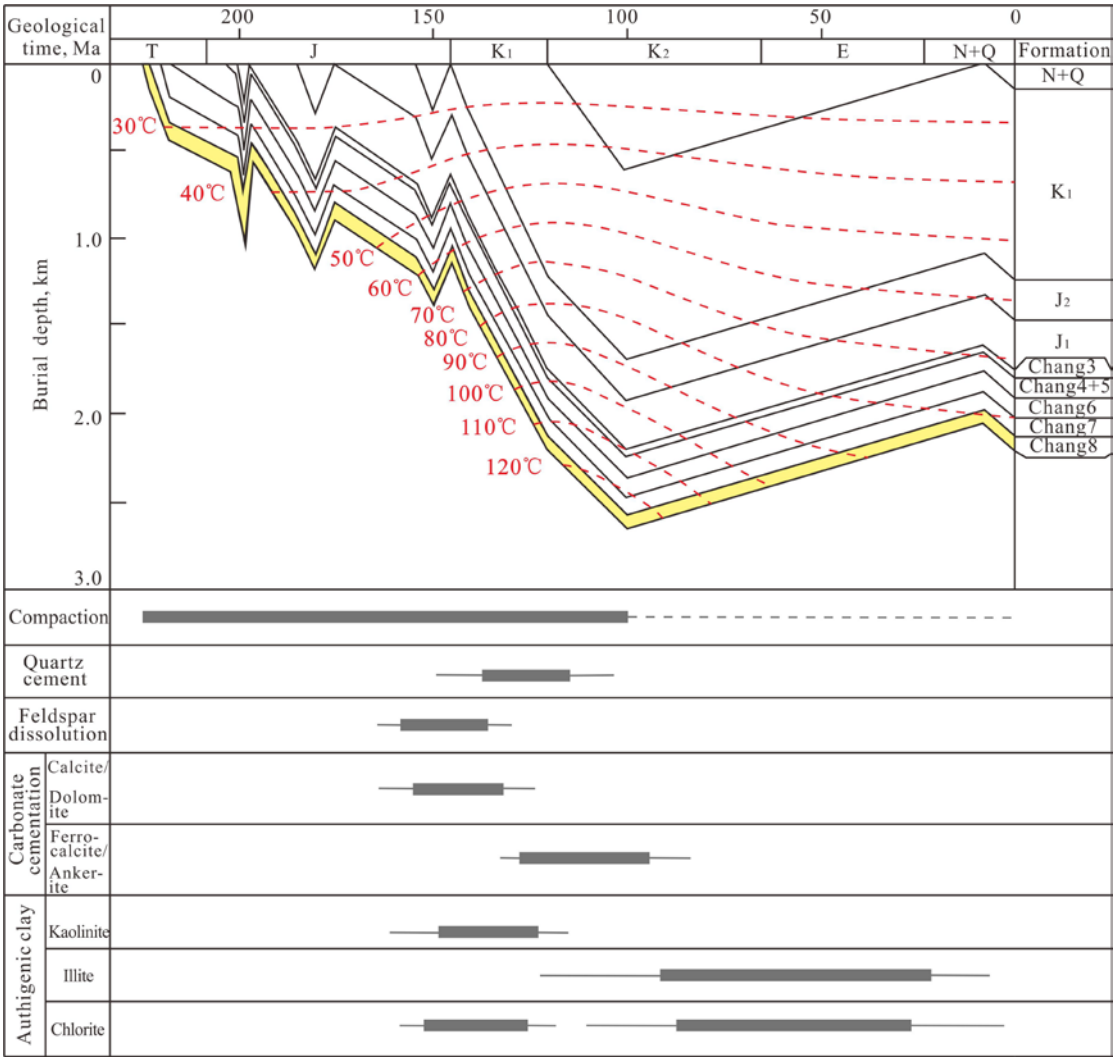

937

938 **Figure 14.** Burial-thermal history and diagenetic sequence of the Chang 8 Member

939 tight sandstone reservoirs in Xifeng Area.

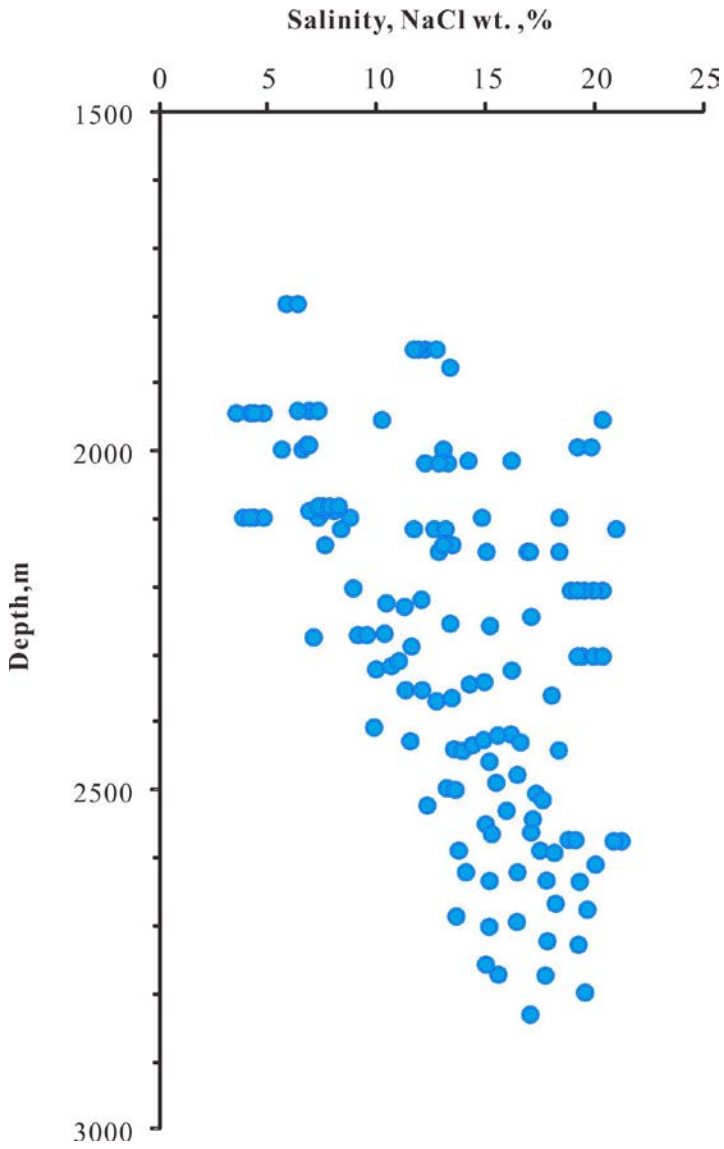

940

941 **Figure 15.** Vertical variation of salinity from ice melting temperature of aqueous fluid

942 inclusions of Chang 8 Member tight sandstone in Xifeng Area.

943

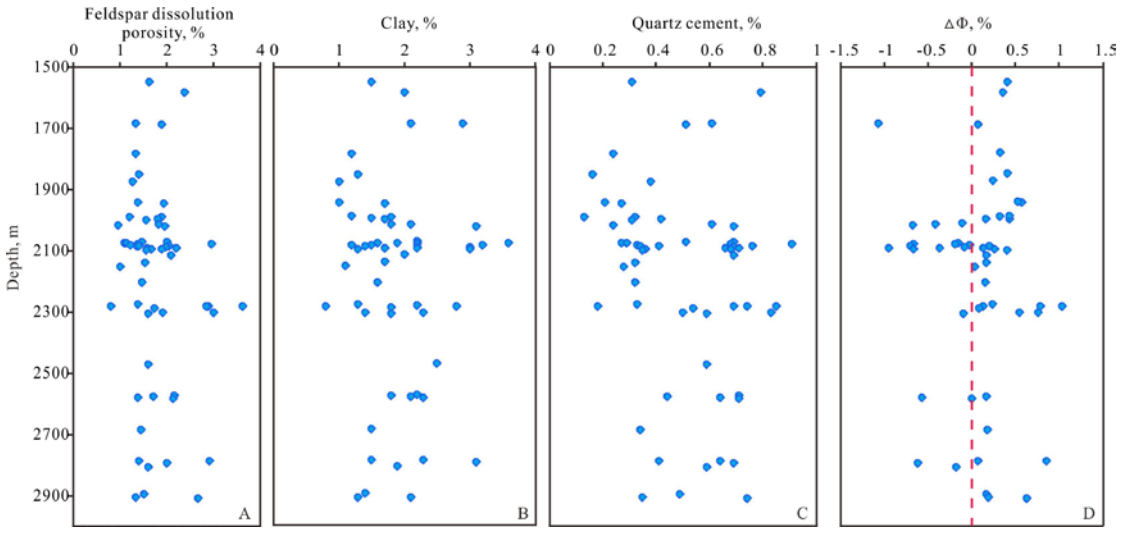

Figure 16. The vertical distribution of the content of feldspar dissolution porosity (A), clay (B) and quartz cement (C) and their difference values (D) in thin section of Chang 8 Member tight sandstone in Xifeng Area. △Φ- Difference values between feldspar dissolution porosity and feldspar dissolved byproducts (The calculation method was described by Yuan et al. 2015b).

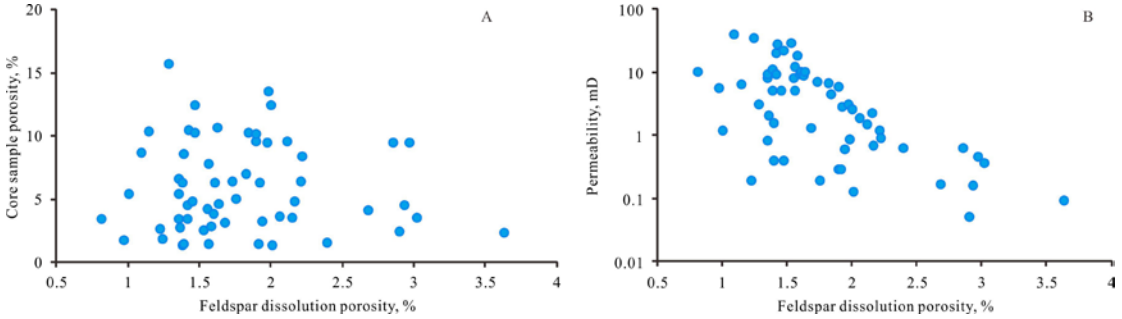

Figure 17. Relationship between the feldspar dissolution porosity, core sample porosity (A) and core sample permeability (B) in Chang 8 Member tight sandstone in Xifeng Area.